Cover sheet for EarthArXiv preprint

Title: Branch-resolved fixed-band near-constant-Q criteria for variable-order fractional seismic attenuation

Authors: Ning Hu, Shuqun Li, Chuyang Hu, and Jiayan Sun

Affiliations and email addresses

Author	Affiliation	Email
Ning Hu	School of Mechanical Engineering, Hangzhou Dianzi University, Hangzhou, China	jluhooning@163.com
Shuqun Li	School of Mathematics and Physics, Xi'an Jiaotong-Liverpool University, Suzhou, China	Shuqun.Li24@student.xjtlu.edu.cn
Chuyang Hu	Department of Computer Science and Engineering, University of California, Santa Cruz, CA 95064, USA	chu207@ucsc.edu
Jiayan Sun	School of Mathematics and Physics, Wenzhou University, Wenzhou, China	susieee6sun@hotmail.com

Peer-review status

This manuscript is a non-peer-reviewed preprint submitted to EarthArXiv. It has been prepared for submission to Geophysical Journal International for peer review.

Mastodon handle: Not provided.

Branch-resolved fixed-band near-constant-Q criteria for variable-order fractional seismic attenuation

Ning Hu[1,*] Shuqun Li[2] Chuyang Hu[3] Jiayan Sun[4]

[1]School of Mechanical Engineering, Hangzhou Dianzi University, Hangzhou, China
[2]School of Mathematics and Physics, Xi'an Jiaotong-Liverpool University, Suzhou, China
[3]Department of Computer Science and Engineering, University of California, Santa Cruz, CA 95064, USA
[4]School of Mathematics and Physics, Wenzhou University, Wenzhou, China

[*]Corresponding author: Ning Hu, `jluhooning@163.com`
E-mail addresses: `Shuqun.Li24@student.xjtlu.edu.cn` (S.L.); `chu207@ucsc.edu` (C.H.)
`susieee6sun@hotmail.com` (J.S.)

July 18, 2026

Abstract

We establish a closed-corridor near-constant-Q criterion for variable-order fractional wave operators. In one-dimensional graded media, and in a conditional multidimensional weak-attenuation corridor assuming a standard caustic-free real geometric-optics phase, the branch-normalized local quality factor satisfies

$$Q(x,\omega) = Q_0(x) + R(x,\omega), \qquad \|R\|_{L^\infty(U\times[\omega_1,\omega_2])} \leq C\left(\|\nabla\alpha\|_\infty + \|\nabla\beta\|_\infty\right)$$

on each fixed frequency band. The operator studied is

$$L_{\alpha,\beta} = {}^C D_t^{\alpha(x)} + c^2(x)(-\Delta)^{\beta(x)/2}.$$

This is a fixed-band admissibility theorem, not a universal all-frequency or global variable-order wave-propagation theorem. Its frozen dispersion relation has a distinguished causal-passive logarithmic branch. On this branch the quality factor is exactly frequency independent, the orders producing a prescribed Q_0 form an explicit one-parameter manifold, and the pair (α,β) is identifiable when attenuation is combined with the velocity-dispersion exponent. The spatial order is interpreted here as an effective phenomenological coordinate for nonlocal dispersion, not as an independent rock-physics state variable; the causal branch is Kramers–Kronig compatible and the high-Q reference remains close to the classical $\beta_{\text{eff}} \approx 2$ regime. The constant in the estimate depends on the band, the passive-cone margin and the scale separation between wavelength and order variation, so the estimate is local in phase space rather than all-frequency. The general multidimensional WKB calculation is used only as a conditional reduction: it identifies the variable-order logarithmic source once a caustic-free complex phase and a controlled lower-order remainder have been supplied. The result is not intended for multipathing, caustics, sharp order jumps, strongly scattering geological structures, or field-scale global propagation without an additional transmission and parametrix theory. The only variable-order source of frequency dependence is the logarithmic derivative of the spatial symbol. Replacing the orders by regional averages incurs a frozen-Q error of $O(\operatorname{osc}\alpha+\operatorname{osc}\beta)$ and can therefore produce order-one errors across sharp contrasts; the corresponding field transfer is conditional, and a nonlocal transmission theorem remains open. Controlled spectral, plane-wave, reduced two-dimensional, and nonseparable small-grid diagnostics test the frozen formula, gradient scaling, averaged-order mechanism, and identifiability. They are finite-dimensional diagnostics, not continuum convergence or field validation. The result provides a geophysical criterion for when smooth heterogeneous fractional orders can be interpreted as a local near-constant-Q model and when regional

averaging is not justified. The numerical experiments are reproducible diagnostics for the formulae and assumptions, not validation of a field-scale propagation model.

Key words: seismic attenuation; wave propagation; fractional wave equation; variable-order operators; WKB analysis.

1 Introduction

1.1 Background and motivation

Seismic waves lose energy as they propagate, and many crustal and exploration-scale analyses treat the quality factor Q as approximately frequency independent over the seismic band. Kjartansson's (1979) constant-Q model gives a causal power-law description of this regime and motivates fractional wave equations for attenuating media. Two related formulations are central for the present work: fractional time-derivative models (Carcione et al., 2002) and the decoupled fractional-Laplacian formulation of Zhu and Harris (2014), which separates amplitude loss from phase delay using two fractional Laplacian terms whose orders depend on the local Q.

The operator studied here is not claimed to be an algebraic rewriting of the Zhu-Harris decoupled fractional-Laplacian equation. Zhu and Harris use a spatially decoupled construction designed to separate amplitude attenuation and phase dispersion, whereas (1) couples a Caputo time-fractional order with a variable-order spatial fractional Laplacian. We use Zhu-Harris as the modelling motivation for averaged fractional-order practice and for the known difficulty of heterogeneous attenuation, but the admissibility condition $\alpha+\beta > 2$ and the two-order manifold derived below belong to the present space-time fractional model. This distinction is important when interpreting the averaged-order error in Section 6: the estimate diagnoses the loss incurred by averaging the orders of (1), not a proof of failure for every Zhu-Harris parametrization.

The physical interpretation is deliberately narrower than a full rock-physics constitutive law. The order α parameterizes temporal memory and intrinsic attenuation, while β parameterizes effective spatial nonlocality and the departure of the attenuation–dispersion pair from the local $\beta = 2$ reference. Thus β is a phenomenological modelling coordinate, not an independently measurable material state variable and not a direct microscopic scattering mechanism. All frozen branches used below are selected by passivity, forward propagation, and Kramers–Kronig compatibility, in the spirit of causal power-law and constant-Q attenuation theories (Caputo, 1967; Kjartansson, 1979; Szabo, 1994; Holm and Näsholm, 2011). Departures from $\beta = 2$ should therefore be read as effective constitutive or dispersion departures rather than as a geometric-scattering closure.

In a homogeneous medium the orders are constant and the theory is classical. Real media are heterogeneous: $Q = Q(x)$, and therefore the fractional orders become variable, $\alpha = \alpha(x)$ and $\beta = \beta(x)$. Here a practical and theoretical difficulty appears. Genuinely x-dependent orders make the operator a variable-order pseudodifferential operator, whose Fourier-side implementation is hampered by Gibbs-type artefacts; to sidestep this, practitioners commonly replace variable orders by regional averages (Zhu and Harris, 2014). As a consequence, the variable-order near-constant-Q regime–the very object that the name VO-NCQ refers to–has remained a heuristic, without a theorem stating when, and how accurately, a variable-order operator realizes a (nearly) frequency-independent Q.

Near-constant-Q dissipative models are well developed in geophysics, from Kjartansson's power-law Q (Kjartansson, 1979) through fractional-derivative, fractional-Zener and fractional-Laplacian wave equations (Carcione et al., 2002; Chen and Holm, 2004; Treeby and Cox, 2010; Zhu and Carcione, 2014; Zhu and Harris, 2014). Numerical modelling of attenuation and viscoelastic wave propagation has an equally substantial background (Robertsson et al., 1994;

Tonn, 1991), while fractional wave theory, inhomogeneous fractional diffusion, and Mittag–Leffler response functions are standard tools for memory-driven dynamics (Chechkin et al., 2005; Gorenflo et al., 2020). These works design, interpret, or compute attenuating wave models whose Q is exactly or approximately frequency independent in prescribed regimes. They do not, however, quantify how a genuinely x-dependent fractional order changes the local frequency dependence of Q. On the mathematical side, variable-order differentiation goes back at least to Samko and Ross (1993), Lorenzo and Hartley (2002), Coimbra (2003), and Sun et al. (2009); variable-order Besov and pseudodifferential constructions are treated by Leopold (1989) and Leopold and Schrohe (1993); and the variable-order fractional Laplacian has recently been given a rigorous real-space definition by Darve et al. (2022). The fixed-order fractional Laplacian itself admits several equivalent analytic realizations (Caffarelli and Silvestre, 2007; Kwaśnicki, 2017), and the well-posedness and regularity of variable-order fractional wave equations have been studied by Jia et al. (2025). None of these addresses the precise relation between the order functions (α, β) and the frequency dependence of the local quality factor.

Our contribution is thus not the constant-Q model–which is classical–but a branch-resolved and microlocal frequency-dependence analysis of the variable-order operator: the exact frozen-coefficient Q-locus and, in particular, a local fixed-band WKB deviation estimate controlling $Q(x, \omega)$ by $\nabla\alpha, \nabla\beta$ under explicit admissibility hypotheses.

1.2 The operator and the main questions

We study the following variable-order space-time fractional operator:

$$L_{\alpha,\beta}u(x,t) := {}^{C}D_t^{\alpha(x)}u(x,t) + c^2(x)(-\Delta)^{\beta(x)/2}u(x,t), \qquad (x,t) \in \Omega \times (0,T), \tag{1}$$

Here $\Omega \subset \mathbb{R}^d$ is a bounded Lipschitz domain, ${}^{C}D_t^{\alpha(x)}$ is the Caputo derivative of x-dependent order $\alpha(x) \in (1, 2]$, and $(-\Delta)^{\beta(x)/2}$ is the variable-order fractional Laplacian of order $\beta(x) \in (0, 2)$. We address three questions.

(Q1) In the frozen-coefficient regime, is the quality factor Q frequency independent, and for which (α, β)? What is the locus of orders realizing a prescribed Q_0?

(Q2) When the orders vary in space, by how much does $Q(x, \omega)$ deviate from frequency independence, and how is the deviation controlled by $\nabla\alpha, \nabla\beta$?

(Q3) What is the modelling error incurred by replacing the variable orders with regional averages?

1.3 Main results and organization

Reader's map. The argument has five gates. First, Section 3 fixes the frozen dispersion relation and the branch-normalized definition of Q. Second, Section 4 proves that only the causal-passive logarithmic branch gives forward attenuation and a Kramers–Kronig compatible lossless limit. Third, the same section shows that fixed Q_0 is a one-parameter two-order manifold and that attenuation alone is therefore non-identifying. Fourth, Section 5 turns on smooth spatial variation and proves a fixed-band WKB corridor in which the departure $Q - Q_0$ is controlled uniformly by the order gradients. Fifth, Section 6 explains why replacing variable orders by regional averages is safe only when the order oscillation is small.

Main result. On any interior region $U \Subset \Omega$ and any fixed frequency band, a smoothly varying variable-order operator realizes a near-constant Q to first order in the order gradients:

$$Q(x,\omega) = Q_0(x) + R(x,\omega), \qquad \|R\|_{L^\infty(U\times[\omega_1,\omega_2])} \le C\big(\|\nabla\alpha\|_\infty + \|\nabla\beta\|_\infty\big)$$

(Proposition 5.5), the variable-order identity $\partial_{x_j}\langle\xi\rangle^{\beta(x)} = (\partial_{x_j}\beta)\log\langle\xi\rangle\,\langle\xi\rangle^{\beta(x)}$ being the sole source of the frequency dependence. This proposition is a conditional WKB reduction, not a stand-alone multidimensional parametrix theorem. The estimate is closed without an additional phase hypothesis in one dimension and conditionally closed, in any dimension, in the weak-attenuation regime once a standard real caustic-free geometric-optics phase is supplied (Theorem 5.15). Two consequences make it usable: the constant-Q orders are *identifiable* from attenuation and dispersion (Proposition 4.14), and the averaged-order approximation has an $O(\operatorname{osc}\alpha+\operatorname{osc}\beta)$ frozen-Q error, with a conditional nonresonant resolvent transfer once the common-space operator comparison (44) is available (Consequence 6.1 and Proposition 6.4).

Practical interpretation and boundary. The closed criterion gives a local diagnostic for a smooth heterogeneous medium over a prescribed seismic frequency band: small spatial gradients of the two orders imply a proportionally small departure from the frozen constant-Q law in the corridors stated in Theorem 5.15. It does not provide a global expansion through caustics, multipathing, boundary layers, strongly scattering structures, or sharp order jumps, and it does not validate a field-scale inversion. In one dimension the required complex phase is constructed directly; in several dimensions the result is conditional on the stated caustic-free geometric-optics input.

In detail. Our answer to (Q1) is Proposition 4.4: in the frozen regime, Q is exactly frequency independent for every admissible (α,β), the quality factor is the explicit function (10), and the constant-Q locus is the manifold (11). We stress, in the interest of honesty about novelty, that the exact constant-Q property is the analytic content of Kjartansson's power law; the novelty in this part is the explicit two-order manifold and the branch-resolved derivation (Lemma 4.1). The genuinely new result is the closed near-constant-Q criterion collected in Theorem 5.15, with a one-dimensional graded-order construction and a weak-attenuation multidimensional corridor. Proposition 5.5 supplies the conditional microlocal reduction behind this criterion: once a caustic-free complex phase and controlled lower-order remainder are available, the only variable-order source entering the leading quality-factor deviation is the logarithmic derivative of the order. The averaged-order consequence (Consequence 6.1) answers (Q3). The frequency-domain field these statements describe is assumed in a nonresonant Fredholm realization (Hypothesis 2.7). A further contribution, of applied interest, is the identifiability result of Section 4.5 (Propositions 4.12 and 4.14): on the constant-Q manifold the pair (α,β) is recovered from the attenuation angle and the velocity dispersion, so the two-order degeneracy becomes a constructive inverse-problem recipe.

The results and their logical status are summarized below.

Question	Result(s)	Status
(Q1) frozen Q, two-order manifold, identifiability	Prop. 4.4; Cons. 4.9; Props. 4.12 and 4.14	exact, closed
(Q2) deviation $\lvert Q-Q_0\rvert \lesssim \lVert\nabla\alpha\rVert_\infty + \lVert\nabla\beta\rVert_\infty$	Thm. 5.15; Prop. 5.5	closed in listed corridors; conditional reduction separated
one dimension, graded order	Lemma 5.9, Cor. 5.10	unconditional
weak attenuation, any d (real GO phase)	Prop. 5.12, Theorem 5.15	conditional on real caustic-free GO
(Q3) averaged-order modelling error	Consequence 6.1	exact; $O(1)$ at interfaces
frequency-domain nonresonance	Hypothesis 2.7	assumed Fredholm realization

Claim	Assumption	Mathematical output	Geophysical meaning
Branch-resolved frozen Q	Passive cone, causal logarithmic branch	Unique forward attenuating branch; exact Q_0	Only the selected branch is a physical attenuation law.
Two-order constant-Q manifold	$1<\alpha<2$, $0<\beta<2$, $\alpha+\beta>2$	Smooth one-dimensional manifold	Q alone does not identify both orders.
Identifiability	Attenuation angle plus dispersion slope	Explicit inverse for (α,β)	Dispersion data are needed to break the trade-off.
Fixed-band WKB corridor	Branch margin, caustic-free phase, wavenumber floor	Uniform $Q-Q_0$ bound on $[\omega_1,\omega_2]$	Smooth local media can be screened for near-constant-Q use.
Averaged-order error	Compact admissible order range	$O(\operatorname{osc}\alpha+\operatorname{osc}\beta)$ frozen-Q error	Regional averaging can fail at sharp contrasts.

What is not proved. We do not prove an all-frequency constant-Q theorem, a global parametrix through caustics, a nonlocal transmission theorem for sharp order jumps, uniqueness of a full inverse problem, convergence of a field-scale numerical solver, or equivalence among all possible definitions of the variable-order fractional Laplacian. The theorem is a local, fixed-band admissibility criterion for the operator and branch stated above. For transparency, the technical inputs that often remain implicit in WKB arguments are stated separately below: branch margin, fixed-band logarithmic remainder control, frozen-symbol perturbation, constant-Q manifold regularity, attenuation-only non-identifiability, one-dimensional phase construction, and weak-attenuation remainder control. This separation is intended to make the proof contract auditable by both mathematical and geophysical readers.

Section 2 fixes notation and recalls the variable-order symbol estimates used here. Section 3 derives the dispersion relation and defines Q. Section 4 gives the exact constant-Q proposition and studies the manifold. Section 5 establishes the local WKB deviation theorem and proves its one-dimensional graded-order instance. Section 6 treats the averaged-order error. Section 7 reports the numerical experiments, including a new nonseparable two-dimensional scattering diagnostic. Section 8 discusses extensions and open problems.

2 Notation and preliminaries

Throughout, $\Omega \subset \mathbb{R}^d$ is a bounded Lipschitz domain and $T>0$. We write $\langle\xi\rangle = (1+|\xi|^2)^{1/2}$ and denote by ω_d the volume of the unit ball in $\mathbb{R}^d$. The orders satisfy the following standing assumption.

Assumption 2.1. $\alpha \in C^1(\Omega)$ with $1 < \alpha_- \le \alpha(x) \le \alpha_+ < 2$; $\beta \in C^1(\Omega)$ with $0 < \beta_- \le \beta(x) \le \beta_+ < 2$; $c \in C^1(\Omega)$ with $0 < c_- \le c(x) \le c_+$. In addition we require the admissibility condition

$$\alpha(x) + \beta(x) > 2 \quad \text{for all } x \in \overline{\Omega}, \qquad \text{implied in particular by } \alpha_- + \beta_- > 2. \tag{2}$$

This is necessary and sufficient for passivity: it ensures $\phi_0(x) = \pi(2-\alpha(x))/(2\beta(x)) \in (0, \pi/2)$ for every x (Lemma 4.1), which is the condition $\kappa_I(x) > 0$ (forward propagation with positive spatial decay). In the boundary cases: $\alpha(x) + \beta(x) \downarrow 2$ gives $\phi_0 \uparrow \pi/2$, $Q_0 \downarrow 0$ (overdamped); $\alpha \uparrow 2$ gives $\phi_0 \downarrow 0$, $Q_0 \to \infty$ (lossless). The strict bound $\alpha_+ < 2$ keeps the model strictly dissipative (so that $\sin(\alpha(x)\pi/2)$ is bounded below and Hypothesis 2.7 applies); the lossless boundary $\alpha = 2$ lies outside Assumption 2.1 and is recorded only as a limiting case in Examples 4.4 and 4.6. All numerical experiments use parameter pairs satisfying (2).

Remark 2.2 (nondimensional reference scales). All symbols in this paper are written after fixing a reference time scale T_0 and length scale L_0. Equivalently, the frozen dispersion relation is

$$(-i\omega T_0)^{\alpha(x)} + \tilde{c}^2(x)(|\xi|L_0)^{\beta(x)} = 0,$$

and the notation below suppresses the tildes. Thus ω, ξ, and c are normalized quantities. For example, a seismic reference frequency $f_0 = 10$ Hz gives $T_0 = 1/f_0 = 0.1$ s; with a reference velocity $v_0 = 3000$ m s^{-1} one may take $L_0 = v_0 T_0 = 300$ m. A physical angular frequency $2\pi f$ is then represented by ωT_0, and a physical wavenumber by $|\xi|L_0$. Without this convention the physical dimension of $c^2(x)$ would vary with $\alpha(x)$ and $\beta(x)$, since ${}^C D_t^{\alpha(x)}$ has dimension $T^{-\alpha(x)}$ and $(-\Delta)^{\beta(x)/2}$ has dimension $L^{-\beta(x)}$. In a dimensional implementation the corresponding coefficient would have units $L^\beta T^{-\alpha}$; the present $c^2(x)$ is its nondimensional counterpart.

2.1 The variable-order Caputo derivative

For $1 < \alpha \le 2$ the Caputo derivative of a function $g \in C^2[0,T]$ is

$${}^C D_t^\alpha g(t) = \frac{1}{\Gamma(2-\alpha)} \int_0^t (t-s)^{1-\alpha} g''(s)\, ds.$$

In (1) the order is the value $\alpha(x)$ frozen at the spatial point x, so for each fixed x the temporal operator is an ordinary Caputo derivative of constant order. For a steady-state time-harmonic field $e^{-i\omega t}$ one has, in the causal stationary regime (the initial Caputo transient decaying), the symbol

$${}^C D_t^\alpha e^{-i\omega t} = (-i\omega)^\alpha e^{-i\omega t}, \qquad \omega > 0, \tag{3}$$

with the principal branch of $(-i\omega)^\alpha$; see Section 3.

2.2 The variable-order fractional Laplacian and symbol class

The variable-order fractional Laplacian is treated microlocally as the pseudodifferential operator with x-dependent symbol $c^2(x)|\xi|^{\beta(x)}$. Related real-space and variable-order pseudodifferential constructions are discussed by Leopold (1989), Leopold and Schrohe (1993), Darve et al. (2022), Hörmander (2007), Shubin (2001), and Stein (1993). The only symbol estimates used in this paper are stated explicitly below and proved in Appendix A. All results below are interior and microlocal ($U \Subset \Omega$) and do not depend on the particular self-adjoint boundary realization of $(-\Delta)^{\beta(x)/2}$ on Ω (Dirichlet, spectral, or restricted); the boundary enters only through the numerical absorbing layers of Section 7. The operators are evaluated within the interior chart $U \Subset \Omega$ to bypass boundary-induced non-local coupling, so the local parametrix is asserted only away from $\partial\Omega$ and does not specify a global boundary topology for the variable-order operator.

This continuous microlocal realization is not identified with any particular positive-semidefinite spectral projection of a symmetrized Kohn–Nirenberg matrix. Such finite-dimensional projected models may share the frozen principal symbol, but time-exact modal evaluation of a prescribed semidiscrete matrix does not by itself prove spatial convergence to the continuous nonsymmetric Kohn–Nirenberg realization analysed here. No convergence bridge is claimed in the present paper.

Definition 2.3. A symbol $a \in C^\infty(\Omega \times \mathbb{R}^d)$ belongs to $S^{\beta(\cdot)}_{\mathrm{var}}$ if for all multi-indices γ, δ there is $C_{\gamma\delta}$ with

$$\left|\partial_x^\gamma \partial_\xi^\delta a(x,\xi)\right| \le C_{\gamma\delta} \langle\xi\rangle^{\beta(x)-|\delta|} (\log\langle\xi\rangle)^{|\gamma|}.$$

The two facts we need are the following. The first is the prototype computation; the second is the subordination that makes the log factors harmless.

Lemma 2.4 (Symbol derivative estimate)**.**

$$\partial_x^\gamma \langle\xi\rangle^{\beta(x)} = P_\gamma(x, \log\langle\xi\rangle)\langle\xi\rangle^{\beta(x)},$$

where P_γ is a polynomial of degree $|\gamma|$ in $\log\langle\xi\rangle$ with coefficients polynomial in $\{\partial_x^{\gamma'}\beta\}_{\gamma' \le \gamma}$. In particular, for $|\gamma| = 1$,

$$\partial_{x_j} \langle\xi\rangle^{\beta(x)} = (\partial_{x_j}\beta)(\log\langle\xi\rangle)\langle\xi\rangle^{\beta(x)},$$

so $c^2(x)\langle\xi\rangle^{\beta(x)} \in S^{\beta(\cdot)}_{\mathrm{var}}$. (Proved in Appendix A.)

Lemma 2.5 (log-subordination)**.** *For every $k \ge 0$ and $\varepsilon > 0$,*

$$\langle\xi\rangle^{\beta(x)}(\log\langle\xi\rangle)^k \le \left(\frac{k}{e\varepsilon}\right)^k \langle\xi\rangle^{\beta(x)+\varepsilon},$$

uniformly in x. Consequently $S^{\beta(\cdot)}_{\mathrm{var}} \subset S^{\beta_+ + \varepsilon}_{1,0}$ for every $\varepsilon > 0$; in particular, the classical Calderón-Vaillancourt theorem and the Hörmander-class parametrix theory apply (with an ε-loss in the order), controlling the WKB remainders used in Section 5. (Proved in Appendix A.)

Remark 2.6. The two lemmas above are the only facts from the variable-order symbol calculus used in this paper; their proofs (Appendix A) are elementary and self-contained. A full global calculus for variable-order symbols would be needed for a global theorem beyond the local fixed-band WKB statement of Section 5.

Lemma 2.7 (Fixed-band logarithmic and exponential remainder control)**.** *Let $I = [\omega_1, \omega_2] \Subset (0,\infty)$ and fix a reference $\omega_0 \in I$. Then*

$$L_I := \sup_{\omega \in I} |\log(\omega/\omega_0)| < \infty.$$

Consequently, for every complex perturbation $z(\omega)$ satisfying $\sup_I |z(\omega)| \le \rho$,

$$\sup_{\omega \in I} |e^{z(\omega)} - 1 - z(\omega)| \le \frac{1}{2}\rho^2 e^\rho.$$

In particular, if

$$z(\omega) = a\,\delta\alpha \log(\omega/\omega_0) + b\,\delta\beta \log(\kappa(\omega)/\kappa(\omega_0))$$

on the causal-passive branch and the branch margin of Lemma 4.2 holds, then

$$\sup_{\omega \in I} |e^{z(\omega)} - 1 - z(\omega)| \le C_I \left(|\delta\alpha| + |\delta\beta|\right)^2,$$

where C_I depends on the band, the passive margin and the admissible order ranges, but not on $\omega \in I$.

Proof. The boundedness of L_I follows from compactness of I and positivity of ω_1. Taylor's formula with integral remainder gives

$$e^z - 1 - z = z^2 \int_0^1 (1-s)e^{sz}\, ds,$$

and hence $|e^z - 1 - z| \le |z|^2 e^{|z|}/2$. On the passive branch, $\log \kappa = \log|\kappa| + i\phi$, with ϕ confined to a compact subinterval of $(0, \pi/2)$ by Lemma 4.2; furthermore $\log|\kappa(\omega)/\kappa(\omega_0)| = (\alpha/\beta)\log(\omega/\omega_0)$. The logarithmic factors are therefore uniformly bounded on I, so $\rho \le C_I(|\delta\alpha| + |\delta\beta|)$, giving the final estimate. $\square$

2.3 Frequency-domain realization and well-posedness

The analysis below is local in phase space, but the notation in (18) presupposes a frequency-domain realization of the time-harmonic problem. We separate this analytic convention from the microlocal calculation. For a fixed $\omega > 0$, let

$$P_\omega v := (-i\omega)^{\alpha(x)} v + \mathrm{Op}\Big(c^2(x)|\xi|^{\beta(x)}\Big)\, v. \tag{4}$$

On the interior chart $U \Subset \Omega$ used in Section 5, P_ω is understood as a properly supported pseudodifferential operator with symbol in $S^{\beta(\cdot)}_{\mathrm{var}}$ plus the order-zero complex multiplication term $(-i\omega)^{\alpha(x)}$. Rather than postulate the existence of the time-harmonic field, we record that we use the following nonresonant realization hypothesis for the global frequency-domain field.

Hypothesis 2.8 (frequency-domain realization and nonresonance)**.** For each fixed frequency band used below, the time-harmonic operator

$$P_\omega v := (-i\omega)^{\alpha(x)} v + \mathrm{Op}\Big(c^2(x)|\xi|^{\beta(x)}\Big)\, v$$

is realized on a chosen Dirichlet-type domain as a closed Fredholm operator $P_\omega : V \to V^*$, and the band avoids its discrete resonance set Σ. On compact subbands of $(0,\infty) \setminus \Sigma$ we assume the uniform resolvent estimate

$$\|v\|_V \le C(\omega)\|f\|_{V^*}, \qquad P_\omega v = f.$$

This is a standard nonresonant frequency-domain input for the global field problem, not a consequence of the local symbol estimates alone. The microlocal WKB calculation in Section 5 uses only the interior symbol and is independent of which self-adjoint or sectorial boundary realization ultimately verifies this hypothesis.

Lemma 2.9 (self-contained high-frequency parametrix estimate)**.** *The a priori estimate*

$$\|u\|_V \le C\big(\|\mathcal{L}_\beta u\|_{V^*} + \|u\|_H\big)$$

used above can be obtained from Lemmas 2.4–2.5 at the level needed here. Let ρ be a smooth high-frequency cutoff with $\rho \equiv 1$ for $|\xi| \ge 2R$ and $\rho \equiv 0$ for $|\xi| \le R$, and set

$$q_0(x,\xi) := \rho(\xi)\big(c^2(x)\langle\xi\rangle^{\beta(x)}\big)^{-1}.$$

Then $q_0 \in S^{-\beta(\cdot)}_{\mathrm{var}}$. The Kohn–Nirenberg product gives

$$q_0 \# \big(c^2\langle\xi\rangle^{\beta(x)}\big) = 1 - \rho_0 + r_1,$$

where ρ_0 is supported in $\{|\xi| \le 2R\}$ and $r_1 \in S^{-1+\varepsilon}_{1,0}$ for every fixed $\varepsilon > 0$. The logarithmic factors generated by x-derivatives of β are precisely those controlled by Lemmas 2.4–2.5. Iterating the remainder gives, modulo an arbitrarily smoothing operator,

$$E = \mathrm{Op}(q_0) \sum_{j=0}^{N-1} \mathrm{Op}(-r_1)^j, \qquad E\mathcal{L}_\beta = \mathrm{Id} + K_N.$$

Choosing N large enough makes K_N compact from V to itself. Standard absorption of the compact remainder and the low-frequency cutoff gives the displayed estimate. This argument is local in charts; a partition of unity and the Dirichlet form realization provide the corresponding bounded-domain estimate.

The local formulas of Section 5 — the branch, the transport equation, and the estimate for $Q(x,\omega)$ — are interior statements about the symbol of P_ω and are independent of the particular boundary realization; Hypothesis 2.7 records the nonresonant global field realization used to interpret the local formulas. Well-posedness of the underlying time-domain Caputo evolution is treated by Jia et al. (2025).

3 The dispersion relation and the quality factor

3.1 Frozen-coefficient dispersion relation

Fix a point x_0 and freeze the coefficients there, writing $\alpha = \alpha(x_0)$, $\beta = \beta(x_0)$, $c = c(x_0)$. We seek a time-harmonic plane-wave solution $u(x,t) = e^{i(\kappa n\cdot x - \omega t)}$ of $L_{\alpha,\beta} u = 0$, where n is a unit direction, $\omega > 0$ is the (real) angular frequency, and $\kappa \in \mathbb{C}$ is the complex wavenumber. Using (3) and $(-\Delta)^{\beta/2} e^{i\kappa n\cdot x} = \kappa^\beta e^{i\kappa n\cdot x}$ (principal branch along the propagation direction), substitution yields the dispersion relation

$$(-i\omega)^\alpha + c^2\kappa^\beta = 0, \qquad \text{equivalently} \qquad \kappa^\beta = -\frac{(-i\omega)^\alpha}{c^2}. \tag{5}$$

Since κ is complex (an attenuating wave), $e^{i\kappa n\cdot x}$ grows or decays exponentially and is not an L^2 eigenfunction; (5) is therefore the dispersion relation of the frozen constant-coefficient *symbol*, not an operator identity on Ω, and the multivalued κ^β is assigned by the causal branch of Lemma 4.1 (Section 4.1) via analytic continuation from $\operatorname{Im}\omega > 0$.

3.2 Definition of the quality factor

Write $\kappa = \kappa_R + i\kappa_I$. For a wave $e^{i(\kappa x - \omega t)}$ travelling in the $+x$ direction, κ_R governs the phase velocity and κ_I the spatial decay. The quality factor is defined by

$$Q := \frac{\kappa_R}{2\kappa_I}, \qquad \text{equivalently} \qquad Q^{-1} = 2\tan\phi, \quad \phi := \arg\kappa. \tag{6}$$

Physical (passive, forward-propagating) waves require $\kappa_R > 0$ and $\kappa_I > 0$, i.e. $\phi \in (0, \pi/2)$, whence $Q > 0$.

4 Exact constant-Q and the two-order manifold

4.1 Branch selection

The relation (5) determines κ^β but leaves a logarithmic branch choice for κ. Because β is not assumed to be an integer, it is not correct to speak of a finite set of β roots. We instead fix a branch of the complex logarithm and select the physically admissible branch of the resulting fractional power.

Lemma 4.1 (Causal-passive branch)**.** *Let $1 < \alpha < 2$, $0 < \beta < 2$, and $\alpha + \beta > 2$. Write*

$$\theta := \pi - \frac{\alpha\pi}{2} \in \left(0, \frac{\pi}{2}\right).$$

For each integer logarithmic branch index $j \in \mathbb{Z}$, the corresponding branch candidate has argument

$$\phi_j = \frac{\pi - \alpha\pi/2}{\beta} + \frac{2\pi j}{\beta}, \qquad j \in \mathbb{Z},$$

where the fractional power is interpreted through $\kappa^\beta = \exp(\beta \operatorname{Log}_j \kappa)$. Among these branch candidates, the unique one satisfying (i) passivity and forward propagation $\phi \in (0, \pi/2)$, (ii) the lossless limit $\phi \to 0$ as $\alpha \to 2$, and (iii) causality ($\kappa(\omega)$ analytic in the upper half-plane, Kramers-Kronig), is the principal branch $j = 0$,

$$\phi = \frac{\pi - \alpha\pi/2}{\beta} \in \left(0, \frac{\pi}{2}\right). \tag{7}$$

Proof. We use the principal branch for the causal temporal symbol. Since $\omega > 0$, $(-i\omega)^\alpha = \omega^\alpha e^{-i\alpha\pi/2}$, so

$$-(-i\omega)^\alpha = \omega^\alpha e^{i(\pi - \alpha\pi/2)},$$

because $-1 = e^{i\pi}$. The argument $\theta := \pi - \alpha\pi/2$ lies in $(0, \pi/2)$ for $1 < \alpha < 2$. On the logarithmic branch indexed by j, write $\kappa = |\kappa| e^{i\phi}$ and $\operatorname{Log}_j \kappa = \log|\kappa| + i(\phi + 2\pi j)$. The equation $\kappa^\beta = (\omega^\alpha/c^2)e^{i\theta}$ then gives $|\kappa| = (\omega^\alpha/c^2)^{1/\beta}$ and $\beta(\phi + 2\pi j) = \theta$ modulo the chosen logarithmic determination. Equivalently, the branch candidates for the physical argument can be written as $\phi_j = \theta/\beta + 2\pi j/\beta$. For $j = 0$,

$$\phi_0 = \frac{\theta}{\beta} = \frac{\pi(2 - \alpha)}{2\beta}.$$

We verify $\phi_0 \in (0, \pi/2)$ explicitly. The lower bound $\phi_0 > 0$ holds since $\alpha < 2$. For the upper bound: $\phi_0 < \pi/2$ iff $\pi(2 - \alpha)/(2\beta) < \pi/2$ iff $2 - \alpha < \beta$ iff $\alpha + \beta > 2$, which is exactly the admissibility condition (2) of Assumption 2.1. Thus $\phi_0 \in (0, \pi/2)$ holds because and only because $\alpha + \beta > 2$.

For $j \neq 0$, ϕ_j exits $(0, \pi/2)$: since $0 < \beta < 2$, neighbouring branch arguments are separated by $2\pi/\beta > \pi$, so at most one branch can lie in the passive forward cone. The lossless limit $\alpha \to 2$ gives $\theta \to 0$, hence $\phi_0 \to 0$, satisfying (ii); no non-principal branch has this limit. Finally the principal branch of $(-i\omega)^\alpha$, continued from $\operatorname{Im} \omega > 0$, gives the causal Kramers-Kronig-compatible determination of $\kappa(\omega)$; the branch $j = 0$ is the only branch that is simultaneously causal, forward propagating, and dissipative. Uniqueness follows from these three requirements. □

4.1.1 Spatially consistent branch selection

The frozen branch in Lemma 4.1 must be chosen consistently when the orders vary with x. The following observation is used throughout Section 5.

Lemma 4.2 (No branch crossing on admissible compact sets)**.** *Let $U \Subset \Omega$ and suppose that $\alpha, \beta \in C^1(U)$ satisfy*

$$1 < \alpha_- \le \alpha(x) \le \alpha_+ < 2, \qquad 0 < \beta_- \le \beta(x) \le \beta_+ < 2, \qquad \alpha(x) + \beta(x) \ge 2 + \eta \tag{8}$$

for some $\eta > 0$. Then the causal-passive phase

$$\phi_0(x) = \frac{\pi(2-\alpha(x))}{2\beta(x)} \tag{9}$$

is a single C^1 branch on U and remains in a compact subinterval of $(0, \pi/2)$. Consequently $\kappa_R(x,\omega) > 0$ and $\kappa_I(x,\omega) > 0$ for the frozen leading branch, and the branch cannot cross to another logarithmic determination while x varies in U.

Proof. The formula (9) is C^1 because α, β are C^1 and $\beta \geq \beta_- > 0$. The lower bound $\alpha < 2$ gives $\phi_0 > 0$. The quantitative admissibility condition gives $2 - \alpha(x) \leq \beta(x) - \eta$, hence

$$\phi_0(x) \leq \frac{\pi}{2}\left(1 - \frac{\eta}{\beta(x)}\right) \leq \frac{\pi}{2}\left(1 - \frac{\eta}{\beta_+}\right) < \frac{\pi}{2}.$$

Thus $\phi_0(U)$ lies in a compact subinterval of $(0, \pi/2)$. The distance to the boundary of the passive cone is positive, so sufficiently small microlocal corrections in Section 5 do not change the sign of κ_R or κ_I on the fixed compact region. Since neighbouring logarithmic branches are separated by more than π, no continuous path in the passive cone can jump to a different branch. □

Lemma 4.3 (Uniform fixed-band branch margin)**.** *Under the hypotheses of Lemma 4.2 and for any fixed band $I = [\omega_1, \omega_2] \Subset (0, \infty)$, there are constants $m_{\mathrm{br}}, M_{\mathrm{br}} > 0$ such that, on $U \times I$,*

$$m_{\mathrm{br}} \leq |\kappa(x,\omega)| \leq M_{\mathrm{br}}, \qquad \operatorname{dist}\big(\arg\kappa(x,\omega), \{0, \pi/2\}\big) \geq m_{\mathrm{br}},$$

and the causal-passive logarithm $\log\kappa(x,\omega)$ is a single C^1 branch of x and ω. Hence every first-order perturbation whose relative wavenumber size is $< m_{\mathrm{br}}/4$ remains on the same branch.

Proof. The modulus is $|\kappa| = \omega^{\alpha(x)/\beta(x)} c(x)^{-2/\beta(x)}$. Since U is compact, $\omega \in I$, c is bounded above and below, and α, β range in compact admissible intervals, $|\kappa|$ has positive lower and finite upper bounds. Lemma 4.2 places $\arg\kappa = \phi_0(x)$ in a compact subinterval of $(0, \pi/2)$; compactness gives a positive distance to both edges of the passive cone. The formula for κ is C^1 in x and ω on this set, and the positive angular margin prevents crossing the logarithmic cut. A relative perturbation smaller than a fixed fraction of the angular and modulus margin cannot leave the cone, so the branch is stable. □

4.2 The exact constant-Q proposition

Proposition 4.4. *Under Assumption 2.1 and the branch (7), the complex wavenumber is*

$$\kappa(\omega) = \left(\frac{\omega^\alpha}{c^2}\right)^{1/\beta} e^{i\phi}, \qquad \phi = \frac{\pi - \alpha\pi/2}{\beta}$$

independent of ω, so that the quality factor is frequency independent:

$$Q_0 = \frac{1}{2}\cot\left(\frac{\pi - \alpha\pi/2}{\beta}\right), \qquad \partial_\omega Q_0 = 0. \tag{10}$$

Proof. By Lemma 4.1, $\kappa = |\kappa| e^{i\phi}$ with $|\kappa| = (\omega^\alpha/c^2)^{1/\beta}$ and ϕ given by (7). All ω-dependence is carried by the modulus; the argument ϕ does not depend on ω. Hence by (6), $Q_0 = (1/2)\cot\phi$, independent of ω. □

Remark 4.5. Proposition 4.4 expresses analytically the well-known fact that a single power law yields a constant Q (Kjartansson). The point we wish to record precisely is the dependence of Q_0 on both orders, which is the basis for the manifold and for the deviation analysis.

4.3 Limiting cases and consistency

Example 4.6 (Lossless limit)**.** If $\alpha = 2$, then $\phi = 0$ and $Q_0 = +\infty$, so the model is lossless. It reduces to the classical wave operator only when $\beta = 2$; for $0 < \beta < 2$ it remains a conservative, spatially fractional dispersive wave equation.

Example 4.7 (Weak attenuation)**.** For $\alpha = 2 - \delta$ with small $\delta > 0$ and $\beta = 2$, $\phi = \pi\delta/4$ and

$$Q_0 = \frac{1}{2}\cot(\pi\delta/4) \approx \frac{2}{\pi\delta},$$

recovering the weak-attenuation scaling $Q_0 \sim 2/(\pi\delta)$ as the fractional part $\delta \to 0$.

Example 4.8 (Purely spatial fractionality is lossless)**.** Taking $\alpha = 2$ (classical second time derivative, no temporal fractionality) and $\beta < 2$ gives $\phi_0 = \pi(2-2)/(2\beta) = 0$, hence $Q_0 = (1/2)\cot(0) = +\infty$: no attenuation. Indeed, $\alpha = 2$ makes the temporal symbol $(i\omega)^2 = -\omega^2$ real, so $\kappa^\beta = \omega^2/c^2 > 0$ is real-positive, giving $\kappa_I = 0$. Spatial fractionality $\beta < 2$ introduces dispersion (non-linear phase velocity $c_\phi = \omega/\kappa_R = (\omega^{2/\beta-1}/c^{2/\beta})^{-1}$) but not attenuation. Constant-Q attenuation requires $\alpha \in (1, 2)$ (temporal fractionality); a purely spatial fractional Laplacian with $\alpha = 2$ is a dispersive, non-attenuating wave equation. For every $\beta \in (0, 2)$ the inequality $\alpha + \beta > 2$ holds at $\alpha = 2$, but $\phi_0 = 0$ places the model on the lossless boundary, rather than in the interior, of the passive cone.

4.4 The constant-Q manifold

Consequence 4.9. *For a prescribed target $Q_0 > 0$, the set of admissible orders is the explicit one-parameter curve*

$$\beta = \frac{\pi(2-\alpha)}{2\,\mathrm{arccot}(2Q_0)}, \qquad \alpha \in (\alpha_*(Q_0), 2), \tag{11}$$

where the left endpoint

$$\alpha_*(Q_0) := 2 - \frac{4}{\pi}\,\mathrm{arccot}(2Q_0) \in (1, 2) \tag{12}$$

is the value at which $\beta = 2$; only $\alpha > \alpha_*(Q_0)$ keeps $\beta < 2$ within Assumption 2.1.

Proof. By (10), $\phi = \mathrm{arccot}(2Q_0)$; substituting $\phi = (\pi - \alpha\pi/2)/\beta = \pi(2-\alpha)/(2\beta)$ and solving for β gives the formula in (11). The constraint $\beta < 2$ reads $\pi(2-\alpha)/(2\,\mathrm{arccot}(2Q_0)) < 2$, i.e. $\alpha > 2 - (4/\pi)\,\mathrm{arccot}(2Q_0) = \alpha_*(Q_0)$; since $\mathrm{arccot}(2Q_0) \in (0, \pi/2)$ one has $\alpha_* \in (1, 2)$. The admissibility condition $\alpha + \beta > 2$ (2) holds automatically on the curve because $\beta = \pi(2-\alpha)/(2\,\mathrm{arccot}(2Q_0)) > 2 - \alpha$ for $\mathrm{arccot}(2Q_0) < \pi/2$, i.e. for every $Q_0 > 0$. □

Remark 4.10. Equation (11) shows that constant-Q does not determine the pair (α, β) uniquely: there is a one-parameter family realizing any given Q_0, trading temporal against spatial fractionality. This degeneracy is relevant to inverse problems and to the choice of formulation (time-fractional vs. spatial-fractional).

Proposition 4.11 (Regularity and non-degeneracy of the constant-Q manifold)**.** *Fix $Q_0 > 0$ and let*

$$F(\alpha, \beta; Q_0) = \frac{1}{2}\cot\left(\frac{\pi(2-\alpha)}{2\beta}\right) - Q_0.$$

At every admissible point satisfying $F = 0$,

$$\partial_\alpha F = \frac{\pi}{4\beta}\csc^2\left(\frac{\pi(2-\alpha)}{2\beta}\right) \neq 0, \qquad \partial_\beta F = \frac{\pi(2-\alpha)}{4\beta^2}\csc^2\left(\frac{\pi(2-\alpha)}{2\beta}\right) \neq 0.$$

Thus the constant-Q locus is a smooth one-dimensional embedded curve in the admissible set. It may be parametrized by either α or β away from the lossless and passive-cone boundaries, and its branch cannot be continued through $\alpha = 2$ or $\alpha + \beta = 2$ without leaving the strict dissipative model.

Proof. Let $\phi = \pi(2-\alpha)/(2\beta)$. On the admissible set, $\phi \in (0, \pi/2)$, so $\csc^2\phi$ is finite and positive. Differentiating $F = (1/2)\cot\phi - Q_0$ gives

$$\partial_\alpha F = -\frac{1}{2}\csc^2\phi\,\partial_\alpha\phi = \frac{\pi}{4\beta}\csc^2\phi \neq 0,$$

and

$$\partial_\beta F = -\frac{1}{2}\csc^2\phi\,\partial_\beta\phi = \frac{\pi(2-\alpha)}{4\beta^2}\csc^2\phi \neq 0.$$

The implicit-function theorem therefore gives a smooth local curve through every point of $F = 0$. Consequence 4.9 supplies the global explicit parametrization, so the local curves join into the stated embedded one-dimensional manifold. At $\alpha = 2$, $\phi = 0$ and $Q_0 = +\infty$; at $\alpha + \beta = 2$, $\phi = \pi/2$ and $Q_0 = 0$. Both lie outside the strict finite-Q, passive dissipative corridor. $\square$

4.5 Phase velocity, dispersion, and identifiability

Proposition 4.4 records the attenuation content of the frozen branch, namely the frequency-independent Q_0. The same branch also fixes the dispersion, and the two observables together resolve the order degeneracy of Remark 4.9. We make both explicit.

Proposition 4.12 (Phase velocity and automatic causality)**.** *Under Assumption 2.1 and the branch (7), the phase velocity of the frozen plane wave is the pure power law*

$$c_\phi(\omega) = \frac{\omega}{\kappa_R(\omega)} = \frac{c^{2/\beta}}{\cos\phi}\,\omega^{\gamma_d}, \qquad \gamma_d := 1 - \frac{\alpha}{\beta}, \tag{13}$$

with group velocity $c_g = (\beta/\alpha)\,c_\phi$. The attenuation coefficient is

$$\kappa_I(\omega) = c^{-2/\beta}\sin\phi\,\omega^{\alpha/\beta}, \qquad \frac{\kappa_I}{\kappa_R} = \tan\phi \quad \textit{(frequency independent)}, \tag{14}$$

which is exactly the constant-Q statement $Q_0^{-1} = 2\tan\phi$. Moreover the complex wavenumber has the closed form

$$\kappa(\omega) = c^{-2/\beta}\,e^{i\pi/\beta}\,(-i\omega)^{\alpha/\beta}, \tag{15}$$

which is the boundary value of a function analytic in the upper half ω-plane and polynomially bounded. Because $\kappa \sim \omega^{\alpha/\beta}$ grows, κ_R and κ_I are related not by an unsubtracted Hilbert transform but by a Kramers-Kronig dispersion relation with $\lceil\alpha/\beta\rceil$ subtractions; for the pure power law (15) this subtracted relation is equivalent to the frequency-independent phase $\arg\kappa = \phi$, i.e. to (14). In this precise sense constant Q and power-law dispersion are two readings of the single analytic object (15), and are consistent with causality.

Proof. By Proposition 4.4, $\kappa_R = |\kappa|\cos\phi = \omega^{\alpha/\beta}c^{-2/\beta}\cos\phi$ and $\kappa_I = |\kappa|\sin\phi$, giving (14) and, dividing ω by κ_R, the law (13); $c_g = (d\kappa_R/d\omega)^{-1} = (\beta/\alpha)c_\phi$ since $\kappa_R \propto \omega^{\alpha/\beta}$. For (15), $(-i\omega)^{\alpha/\beta} = \omega^{\alpha/\beta}e^{-i\alpha\pi/(2\beta)}$, so the right-hand side has modulus $c^{-2/\beta}\omega^{\alpha/\beta} = |\kappa|$ and argument $\pi/\beta - \alpha\pi/(2\beta) = \pi(2-\alpha)/(2\beta) = \phi$; it therefore equals κ. Analyticity in $\{\Im\omega > 0\}$ is the principal branch of $(-i\omega)^{\alpha/\beta}$ (cut on the negative imaginary axis), which is condition (iii) of Lemma 4.1. $\square$

Remark 4.13. The sign of γ_d is diagnostic: on the manifold (11), $\gamma_d = 0$ iff $\alpha = \beta$ (dispersionless attenuation), $\gamma_d > 0$ iff $\alpha < \beta$ (velocity increases with frequency), and $\gamma_d < 0$ iff $\alpha > \beta$. A genuinely space-time fractional model can therefore carry attenuation with any sign of velocity dispersion, whereas a purely time-fractional model ($\beta = 2$ fixed) ties the two together. This freedom is the physical meaning of the extra order.

We now use the dispersion exponent to remove the degeneracy of Remark 4.9. Write the two frozen observables as

$$\phi = \operatorname{arccot}(2Q_0) \ \ \text{(from attenuation)}, \qquad \gamma_d = 1 - \frac{\alpha}{\beta} \ \ \text{(from phase-velocity dispersion, (13))}.$$

Proposition 4.14 (Identifiability from attenuation and dispersion)**.** *On the admissible set* $\{1 < \alpha < 2,\ 0 < \beta < 2,\ \alpha + \beta > 2\}$ *the map* $(\alpha, \beta) \mapsto (\phi, \gamma_d)$ *is a diffeomorphism onto its image, with Jacobian*

$$\frac{\partial(\phi, \gamma_d)}{\partial(\alpha, \beta)} = -\frac{\pi}{\beta^3} \neq 0, \tag{16}$$

and inverts explicitly by

$$\beta = \frac{\pi}{\phi + \frac{\pi}{2}(1 - \gamma_d)}, \qquad \alpha = (1 - \gamma_d)\,\beta. \tag{17}$$

Consequently a single-frequency Q_0 measurement (which fixes only ϕ) leaves the manifold (11) undetermined, but the pair (Q_0, γ_d)–attenuation together with the dispersion slope–determines (α, β) uniquely.

Proof. With $\phi = \pi(2 - \alpha)/(2\beta)$ and $\gamma_d = 1 - \alpha/\beta$,

$$\partial_\alpha \phi = -\frac{\pi}{2\beta}, \quad \partial_\beta \phi = -\frac{\pi(2-\alpha)}{2\beta^2}, \quad \partial_\alpha \gamma_d = -\frac{1}{\beta}, \quad \partial_\beta \gamma_d = \frac{\alpha}{\beta^2},$$

so the Jacobian determinant is

$$\Big(-\tfrac{\pi}{2\beta}\Big)\Big(\tfrac{\alpha}{\beta^2}\Big) - \Big(-\tfrac{\pi(2-\alpha)}{2\beta^2}\Big)\Big(-\tfrac{1}{\beta}\Big) = -\frac{\pi}{2\beta^3}\big[\alpha + (2-\alpha)\big] = -\frac{\pi}{\beta^3},$$

which is (16). For (17): $\gamma_d = 1 - \alpha/\beta$ gives $\alpha = (1-\gamma_d)\beta$; substituting into $\phi = \pi/\beta - (\pi/2)(\alpha/\beta) = \pi/\beta - (\pi/2)(1-\gamma_d)$ and solving for β gives the first identity, and back-substitution the second. Non-vanishing of (16) makes the map a local diffeomorphism; (17) exhibits a single-valued global inverse on the admissible set. □

Remark 4.15. This is the constructive counterpart of Remark 4.9 and gives a measurement recipe for the inverse problem: extract Q_0 from the amplitude-decay slope and γ_d from the frequency dependence of the phase velocity, then read (α, β) from (17). It also shows which datum breaks the degeneracy–dispersion, not a second attenuation measurement, since any number of Q_0 values at different frequencies return the same ϕ. As a check, $(\alpha, \beta) = (1.9, 1.8)$ gives $\gamma_d = -0.0556$, $\phi = \pi/36$ ($Q_0 = 5.715$), and (17) returns $(\alpha, \beta) = (1.900, 1.800)$; $(1.7, 1.2)$ gives $\gamma_d = -0.4167$, $\phi = 0.3927$ ($Q_0 = 1.207$), and (17) returns $(1.700, 1.200)$–the two layers of Experiment A (Section 7.2).

Proposition 4.16 (Non-identifiability from attenuation alone)**.** *Fix $Q_0 > 0$. Any observation that determines only the frozen attenuation angle $\phi = \operatorname{arccot}(2Q_0)$, including repeated fixed-band estimates of the same frequency-independent Q_0, leaves the one-dimensional family (11) undetermined. Hence (α, β) is not identifiable from Q_0 alone; an additional dispersion observable, branch prior, or model constraint is necessary.*

Proof. Equation (10) shows that Q_0 depends on (α, β) only through $\phi = \pi(2-\alpha)/(2\beta)$. For fixed Q_0, ϕ is fixed and Consequence 4.9 gives the continuum of admissible pairs $\beta = \pi(2-\alpha)/(2\phi)$, $\alpha \in (\alpha_*(Q_0), 2)$. Distinct choices of α in this interval produce distinct (α, β) with the same attenuation angle and therefore the same Q_0 at every frequency. Proposition 4.14 shows that adding the independent dispersion slope γ_d removes this one-dimensional null direction. □

5 Local WKB construction and quality-factor deviation

We now allow the orders to vary in space and quantify the resulting frequency dependence of Q. This section is a microlocal WKB reduction, not a global well-posedness theorem for the full nonlocal boundary-value problem. The estimate is local in phase space, away from caustics and boundary layers, and applies on frequency bands where the solution admits the WKB expansion stated below.

The small quantity is the wavelength-to-heterogeneity ratio on the fixed band. After the nondimensionalization of Section 2, let

$$\varepsilon_{\text{het}} := \sup_U (|\nabla\alpha| + |\nabla\beta| + |\nabla \log c|) \sup_{\omega\in[\omega_1,\omega_2]} |k(x,\omega)|^{-1}.$$

All fixed-band constants below may depend on the passive-cone margin, the coefficient ranges, and the endpoints of the frequency band; the WKB statement is meaningful when $\varepsilon_{\text{het}} \ll 1$. Thus "fixed band" does not mean that an arbitrary heterogeneous field has a small remainder. It means that, on the prescribed seismic band, the order profiles vary slowly relative to the local wavelength and the constants are not claimed to be uniform as the lower endpoint approaches a low-wavenumber regime.

For the quality-factor estimate itself we separate this geometric scale from the intrinsic variable-order source. After the leading real transport gauge has been fixed, variations of c affect ray geometry and amplitude spreading but do not enter the branch angle defining Q_0. The Q-relevant small scale is therefore

$$\varepsilon_{\text{vo}} := \sup_U (|\nabla\alpha| + |\nabla\beta|) \sup_{\omega\in[\omega_1,\omega_2]} |\kappa_0(x,\omega)|^{-1}.$$

The c-dependence remains in the constants through the wavenumber floor, ray Jacobian, and transport inverse.

The logical structure is as follows. Section 5.1 states the local admissibility assumptions needed for a complex WKB expansion. Section 5.2 proves that the variable-order terms enter the first transport equation through logarithmic order-derivative sources and that the symbolic remainder is lower order on a fixed frequency band. Section 5.3 gives a conditional local deviation reduction under these explicit assumptions. Section 5.4 then verifies the assumptions in the one-dimensional graded-order setting used in Experiment B and in a weak-attenuation multidimensional corridor. Thus the unrestricted multidimensional statement is conditional on a caustic-free complex phase and a controlled local-wavenumber remainder, while the one-dimensional graded-order result is a closed theorem within the present paper.

We work in the frequency domain: a time-harmonic field $u(x,t) = v(x,\omega)e^{-i\omega t}$ satisfies

$$(-i\omega)^{\alpha(x)} v + c^2(x)(-\Delta)^{\beta(x)/2} v = 0. \tag{18}$$

5.1 WKB admissibility and local quality factor

Let $U \Subset \Omega$ be an interior region and let $[\omega_1, \omega_2] \subset (0, \infty)$ be the frequency band of interest. We use the following microlocal admissibility hypothesis.

Regularity convention. Throughout this section we take $\alpha, \beta, c \in C^\infty(U)$ for the multidimensional construction; in one dimension $C^1(\overline{U})$ suffices (Lemma 5.9), because the eikonal is then solved by direct integration and no parametrix through caustics is required.

Hypothesis 5.1 (Fixed-band WKB admissibility)**.** On $U \times [\omega_1, \omega_2]$, assume that the frequency-domain solution is microlocally represented by a complex-phase ansatz

$$v(x,\omega) = a(x,\omega)e^{i\omega\psi(x)}, \qquad k(x) := \omega\nabla\psi(x), \tag{19}$$

where $\psi = \psi_R + i\psi_I$ is allowed to be complex, $\psi_I \geq 0$ gives spatial decay, and a is an elliptic amplitude. Equivalently, along a real ray direction $n(x)$ one may write the complex covector as $k(x,\omega) = \kappa(x,\omega)n(x)$, with $\kappa = \kappa_R + i\kappa_I$ on the causal-passive branch. Fractional powers of the complex covector are not obtained by an undefined substitution into a real symbol. The WKB admissibility hypothesis used in Proposition 5.5 consists of the following fixed-band inputs:

(A1) *Passive branch and branch margin.* The calculation is restricted to the passive cone $\kappa_R > 0, \kappa_I > 0$, with a fixed logarithmic branch and positive distance from the branch cut. The notation $|k|$ denotes the elliptic size of this branch-corrected covector, comparable to $|\kappa|$, while $\log\kappa$ denotes the causal-passive complex logarithm fixed in Lemma 4.1 and kept uniform on the band by Lemma 4.3.

(A2) *Caustic-free complex phase.* The phase ψ has no caustic on U; equivalently, the ray Jacobian is bounded with determinant bounded away from zero on the ray tube considered.

(A3) *Positive wavenumber floor.* The branch-corrected covector obeys $|k(x,\omega)| \geq k_{\min} > 0$ on $U \times [\omega_1, \omega_2]$.

(A4) *Transport amplitude gauge.* The elliptic amplitude a is fixed by the leading real transport normalization used in the branch-normalized local-Q definition below.

(A5) *Local-wavenumber remainder bound.* The remainder after the first transport equation is bounded in the variable-order symbol class described in Section 2.2. For the conditional multidimensional reduction only, the branch-corrected local-wavenumber contribution of the lower-order remainder is assumed to be $O(\varepsilon_{\text{het}})$ on the chosen band after the first transport solve.

Clause (A5) is the external WKB admissibility input in Proposition 5.5; it is discharged only in the one-dimensional and weak-attenuation corridors collected in Theorem 5.15. In numerical use, the same hypothesis is checked by a local plane-wave residual gate: if a fitted window has

$$\mathcal{R}_U(\omega) := \frac{\|P_\omega(ae^{i\omega\psi})\|_{L^2(U)}}{\|ae^{i\omega\psi}\|_{L^2(U)}}$$

larger than the prescribed tolerance, the branch-normalized Q estimate is not interpreted by the theorem.

Lemma 5.2 (Frozen-symbol perturbation in a local window)**.** *Let $B_r(x_0) \Subset U$, let $I = [\omega_1, \omega_2] \Subset (0, \infty)$, and assume the fixed-band branch margin of Lemma 4.3. For the principal symbol*

$$p(x,\kappa,\omega) = (-i\omega)^{\alpha(x)} + c^2(x)\kappa^{\beta(x)}$$

evaluated on the causal-passive branch with $|\kappa|$ in the fixed-band compact range, one has

$$\sup_{x\in B_r(x_0),\,\omega\in I} |p(x,\kappa,\omega) - p(x_0,\kappa,\omega)| \leq C_I r \left(\|\nabla\alpha\|_{L^\infty(B_r)} + \|\nabla\beta\|_{L^\infty(B_r)} + \|\nabla \log c\|_{L^\infty(B_r)}\right),$$

after normalization by the principal elliptic size. The constant depends on the fixed band, admissible order ranges, $c_\pm$, and the branch margin, but not on r.

Proof. By the mean-value theorem,

$$|(-i\omega)^{\alpha(x)} - (-i\omega)^{\alpha(x_0)}| \le C_I|\alpha(x) - \alpha(x_0)|$$

because $|\partial_\alpha(-i\omega)^\alpha| = |(-i\omega)^\alpha \log(-i\omega)|$ is uniformly bounded on the fixed band and admissible order interval. Similarly, on the single causal-passive branch,

$$|\kappa^{\beta(x)} - \kappa^{\beta(x_0)}| \le C_I|\beta(x) - \beta(x_0)|,$$

because $\partial_\beta \kappa^\beta = \kappa^\beta \log\kappa$ and $\log\kappa$ is uniformly bounded by Lemmas 4.2 and 4.3. The coefficient factor satisfies $|c^2(x) - c^2(x_0)| \le Cr\|\nabla \log c\|_\infty$ on $B_r(x_0)$. Dividing by the fixed-band elliptic size and using $|\alpha(x) - \alpha(x_0)| \le r\|\nabla\alpha\|_\infty$ and $|\beta(x) - \beta(x_0)| \le r\|\nabla\beta\|_\infty$ gives the estimate. □

The leading eikonal equation is

$$(-i\omega)^{\alpha(x)} + c^2(x)|k(x)|^{\beta(x)} = 0, \tag{20}$$

which is the frozen dispersion relation (5) satisfied pointwise. By Lemma 4.1 it determines the causal-passive local branch.

Definition: branch-normalized local quality factor. For a WKB field $v = a\, e^{i\omega\psi}$ on an admissible ray tube, fix the leading transport gauge by choosing a from the real elliptic transport equation. The branch-normalized scalar wavenumber is the causal-passive scalar component of the gauge-corrected logarithmic derivative,

$$\kappa_{\text{loc}}(x,\omega) := -i\, n(x) \cdot \nabla \log(v(x,\omega)/a(x,\omega)),$$

where $n(x)$ is the ray direction and the logarithm is taken on the spatially consistent passive branch of Lemma 4.2. The corresponding local quality factor is

$$Q(x,\omega) := \frac{\operatorname{Re}\kappa_{\text{loc}}(x,\omega)}{2\ \operatorname{Im}\kappa_{\text{loc}}(x,\omega)}, \qquad \operatorname{Re}\kappa_{\text{loc}} > 0, \quad \operatorname{Im}\kappa_{\text{loc}} > 0.$$

This is the continuum quantity estimated numerically by the windowed plane-wave procedure of Section 7: a window is accepted only when the local residual is small enough that the same branch and gauge can be identified. In frozen coefficients this definition reduces to the following frozen value:

$$Q_0(x) = \frac{1}{2}\cot\left(\frac{\pi - \alpha(x)\pi/2}{\beta(x)}\right).$$

The deviation estimated below is therefore the difference between this branch-normalized $Q(x,\omega)$ and the frozen $Q_0(x)$.

Physical observables represented by the symbols. The branch angle $\phi = \arg\kappa$ is the attenuation angle: $Q^{-1} = 2\tan\phi$ in the frozen model. The real part κ_R determines phase velocity $c_\phi = \omega/\kappa_R$, while the imaginary part κ_I determines amplitude decay along the ray. The dispersion exponent $\gamma_d = d\log c_\phi/d\log\omega$ is therefore an observable slope of phase velocity over the usable band, and the local Q estimate is the slope of logarithmic amplitude decay after branch and transport normalization. The fixed band $[\omega_1, \omega_2]$ represents the part of the seismic spectrum for which these two slopes can be stably estimated; the theorem does not extend those estimates to unobserved frequencies.

5.2 Variable-order transport source and symbolic remainder

The next order in the WKB hierarchy yields the transport equation for the amplitude a. The only terms that distinguish the variable-order problem from an ordinary variable-coefficient problem are the logarithmic derivatives of the orders. In the formulas below q denotes the branch-corrected scalar size of the covector: $q = |\xi|$ on real covectors and $q = \kappa$ on the admissible complex ray $k = \kappa n$. By Lemma 2.4,

$$\partial_{x_j}\left(c^2 q^{\beta(x)}\right) = (\partial_{x_j} c^2) q^\beta + c^2(\partial_{x_j}\beta) q^\beta \log q + \beta c^2 q^{\beta-1}\partial_{x_j} q, \tag{21}$$

$$\partial_{x_j}\left((-i\omega)^{\alpha(x)}\right) = (\partial_{x_j}\alpha)(-i\omega)^\alpha \log(-i\omega). \tag{22}$$

The terms $\log q$ and $\log(-i\omega)$ are the hallmark of variable order (Lemma 2.4). We now *derive* the first transport equation rather than positing it.

Write the principal symbol of (18) as

$$p(x,\xi,\omega) = (-i\omega)^{\alpha(x)} + c^2(x) q(x,\xi)^{\beta(x)},$$

where $q(x,\xi)$ is the branch-corrected scalar size of the covector. On a real covector $q = |\xi|$; on the admissible complex ray $k = \kappa n$, $q(x,k) = \kappa$ and $\log q$ is the causal-passive logarithm fixed in Lemma 4.1. This convention avoids substituting a complex vector into an unbranched real norm. The following local expansion is the symbolic input behind the transport equation.

Lemma 5.3 (Local WKB conjugation and remainder)**.** *Let $U \Subset \Omega$, let $a, \psi \in C^\infty(U)$, and assume that the complex covector $k = \omega\nabla\psi$ remains in the causal-passive branch and satisfies $|k| \geq k_{\min} > 0$ on $U \times [\omega_1, \omega_2]$. For a properly supported Kohn–Nirenberg quantization of p on U, the conjugated operator has the fixed-band expansion*

$$e^{-i\omega\psi}\,\mathrm{Op}(p)\big(a\,e^{i\omega\psi}\big) = p(x,k)\,a + \frac{1}{i}\Big[\partial_\xi p(x,k)\cdot\nabla a + \tfrac{1}{2}\big(\partial^2_{\xi\xi} p(x,k) : \nabla_x k\big)a + p_{\mathrm{sub}}(x,k)\,a\Big] + r, \tag{23}$$

where p_{sub} denotes the quantization-dependent first subprincipal contribution. In Kohn–Nirenberg form it is represented, up to the harmless sign convention absorbed into T_1, by $\frac{1}{2i}\sum_j \partial_{x_j}\partial_{\xi_j} p$. The displayed bracket contains all first-transport terms that can affect the amplitude or the branch-normalized logarithmic derivative. Moreover, for every $\varepsilon > 0$, the second and higher symbolic remainders are bounded on the fixed band by

$$\|r\|_{L^\infty(U)} \leq C_{\varepsilon,U,\omega_1,\omega_2}\left(\|a\|_{C^3(U)} + \|\psi\|_{C^4(U)}\right)\langle k\rangle^{\beta_+ - 2 + \varepsilon}, \tag{24}$$

with the logarithmic losses absorbed into ε by Lemma 2.5. Thus the retained transport terms are one order below the principal eikonal term, while the discarded part is a second-order symbolic remainder relative to the principal symbol.

Proof. The first two displayed levels in (23) are the standard local pseudodifferential expansion of $\mathrm{Op}(p)$ conjugated by $e^{i\omega\psi}$. The first level is the eikonal term $p(x,k)a$. The second level contains the transport operator, including the subprincipal contribution determined by the chosen quantization. The only point specific to the variable-order symbol is the appearance of $\partial_x\alpha$ and $\partial_x\beta$ factors when differentiating the powers $(-i\omega)^{\alpha(x)}$ and $q^{\beta(x)}$. Lemma 2.4 gives the resulting powers of $\log(-i\omega)$ and $\log q$, and Lemma 2.5 subordinates these logarithms to $\langle\xi\rangle^\varepsilon$ on the fixed band. After the first transport level is retained, the remaining symbolic expansion begins two ξ-derivatives below the principal symbol; hence it has order $\beta_+ - 2 + \varepsilon$, which gives (24). $\square$

The principal ($O(1)$) term in (23) is the eikonal (20), $p(x,k)=0$. Vanishing of the bracket is the first transport equation. Its principal advection is elliptic and order-independent,

$$T_0 a := \partial_\xi p(x,k)\cdot\nabla a + \tfrac{1}{2}(\nabla\cdot\partial_\xi p)(x,k)\, a,$$

which reduces to $2k\cdot\nabla a+(\nabla\cdot k)a$ in the classical normalization $\beta=2,\ c\equiv 1$, and is nonzero because the ellipticity factor $\partial_\kappa p=\beta c^2\kappa^{\beta-1}$ does not vanish on the passive cone (Lemma 4.1: $\kappa\neq 0,\ \beta\in(0,2)$). The variable-order contribution is the part of $\partial_x p$ that carries x-derivatives of the *orders*: by (21)-(22) the only terms absent from an ordinary variable-coefficient problem are the two logarithmic ones, $(\partial_{x_j}\alpha)(-i\omega)^\alpha\log(-i\omega)$ and $c^2(\partial_{x_j}\beta)\kappa^\beta\log\kappa$, with $\log\kappa$ evaluated on the passive branch. Dividing the bracket by the ellipticity factor puts the equation in the form

$$T_0 a + T_1(\alpha,\beta,c;k)a = 0, \tag{25}$$

with the variable-order part bounded pointwise by

$$|T_1| \le C(\alpha_\pm,\beta_\pm,c_\pm,\|c\|_{C^1})\left(|\nabla\alpha|\,|\log\omega| + |\nabla\beta|\,|\log\langle k\rangle|\right). \tag{26}$$

The ordinary (non-logarithmic) variable-coefficient terms, including $\partial_x c$ and the geometric-spreading contribution, are absorbed into T_0, into the leading real transport gauge, or into the harmless fixed-band constant C. The two displayed logarithmic terms are the only new order-derivative sources. Finally, by Lemma 2.5 the logarithmic factors remain at transport order after the eikonal term is removed, whereas the discarded symbolic remainder in (24) is two orders below the principal symbol. Hence (25)-(26) is a first transport equation with an explicit variable-order source, not a formal ansatz. The remaining analytic input is the existence of a caustic-free complex phase. Proposition 5.7 records this as a conditional reduction in several dimensions, and Lemma 5.9 proves it directly in one dimension.

5.3 Local fixed-band deviation theorem

Lemma 5.4 (From transport source to local quality-factor correction)**.** *Assume the WKB-admissibility hypothesis on $U\times[\omega_1,\omega_2]$ and let $\kappa_0(x,\omega)$ denote the causal-passive frozen branch determined by (20). Define the branch-corrected local scalar wavenumber by differentiating the normalized complex phase along the ray direction, equivalently by the local logarithmic derivative*

$$\kappa_{\mathrm{loc}}(x,\omega) := -i\,n(x)\cdot\nabla\log v(x,\omega)$$

after subtracting the elliptic amplitude fixed by the leading real transport normalization. Then

$$\kappa_{\mathrm{loc}} = \kappa_0 + \delta\kappa_{\mathrm{vo}} + \delta\kappa_{\mathrm{rem}},$$

where

$$\left|\frac{\delta\kappa_{\mathrm{vo}}(x,\omega)}{\kappa_0(x,\omega)}\right| \le C\left(|\nabla\alpha(x)|\,|\log\omega| + |\nabla\beta(x)|\,|\log\langle\kappa_0\rangle|\right),$$

and, in the conditional multidimensional reduction, the assumed local-wavenumber remainder satisfies

$$\left|\frac{\delta\kappa_{\mathrm{rem}}(x,\omega)}{\kappa_0(x,\omega)}\right| \le C_{\mathrm{WKB}}\left(|\nabla\alpha(x)|\,|\log\omega| + |\nabla\beta(x)|\,|\log\langle\kappa_0\rangle|\right) + C_{\mathrm{WKB}}\frac{\varepsilon_{\mathrm{vo}}}{|\kappa_0(x,\omega)|}$$

on the fixed band. The last term represents the genuinely lower-order symbolic and estimator remainder after the first transport gauge has been fixed. The constants depend on the compact passive-cone margin, the coefficient ranges, the amplitude ellipticity bounds, and the WKB remainder bound. Consequently, on every compact subset of the passive cone,

$$
\begin{aligned}
|R(x,\omega)| &:= |Q(x,\omega) - Q_0(x)| \\
&\leq C\left(|\nabla\alpha(x)|\,|\log\omega| + |\nabla\beta(x)|\,|\log\langle\kappa_0\rangle| + \frac{\varepsilon_{\mathrm{vo}}}{|\kappa_0(x,\omega)|}\right), \qquad (27)\\
|\kappa_0| &= \omega^{\alpha/\beta}c^{-2/\beta}.
\end{aligned}
$$

Proof. The eikonal equation gives the leading scalar wavenumber κ_0. The first transport equation identifies the order-derivative source terms that perturb the branch-normalized logarithmic derivative after the ordinary real amplitude transport has been removed. The order-derivative part of the transport bracket is

$$(\nabla\alpha)(-i\omega)^\alpha \log(-i\omega) + c^2(\nabla\beta)\kappa_0^\beta \log\kappa_0.$$

Using the eikonal identity $(-i\omega)^\alpha = -c^2\kappa_0^\beta$ and dividing by the nonzero ellipticity factor $\partial_\kappa p = \beta c^2\kappa_0^{\beta-1}$ gives

$$\frac{\delta\kappa_{\mathrm{vo}}}{\kappa_0} = O((\nabla\alpha)\log(-i\omega) - (\nabla\beta)\log\kappa_0),$$

which is the calculation written explicitly in Appendix B.2. The term $\delta\kappa_{\mathrm{rem}}$ is not a new theorem in this proposition: it is the remaining WKB-admissibility input for the unrestricted multidimensional reduction and is verified only in the closed corridors below. The lower-order Q-relevant part is divided once more by the local elliptic scale, giving the displayed $\varepsilon_{\mathrm{vo}}/|\kappa_0|$ contribution. Non-logarithmic c-gradient terms have already been absorbed into the real transport gauge and the constants. Finally, the map $z \mapsto \operatorname{Re} z/(2\operatorname{Im} z)$ has bounded derivative with respect to the relative perturbation z/κ_0 on any compact subcone of $\kappa_R > 0, \kappa_I > 0$. The mean-value theorem therefore gives (27). $\square$

Proposition 5.5 (Conditional local fixed-band WKB reduction)**.** *Under Assumption 2.1 and Hypothesis 5.1 on $U \times [\omega_1, \omega_2]$, the local quality factor satisfies $Q(x,\omega) = Q_0(x) + R(x,\omega)$ and*

$$\|R\|_{L^\infty(U\times[\omega_1,\omega_2])} \leq C(\beta_\pm, \alpha_\pm, \omega_1, \omega_2)\left(\|\nabla\alpha\|_\infty + \|\nabla\beta\|_\infty\right), \qquad (28)$$

where the constant contains the band factor $\log(\omega_2/\omega_1)/\inf_{U\times[\omega_1,\omega_2]}|k(x,\omega)|$ and the WKB remainder bound. Thus the proposition is a fixed-band reduction: the constant may deteriorate as the band widens or as the lower endpoint approaches a regime where $\inf|k|$ is small. In particular, for homogeneous orders $R \equiv 0$ at the WKB order considered here, consistently with Proposition 4.4.

Proof. The eikonal equation (20) fixes the leading local branch. By Lemma 4.1 and Lemma 4.2, this branch is causal-passive and spatially consistent on U. The leading local scalar wavenumber therefore has the same phase angle as in the frozen calculation, and the leading quality factor is exactly $Q_0(x)$.

Lemma 5.3 gives the controlled first transport equation and Lemma 5.4 converts its variable-order source into the pointwise correction (27). It remains only to make the logarithmic factors uniform on the band. By Lemma 2.5 with $\langle\xi\rangle \sim |\kappa_0|$, for any $\varepsilon > 0$,

$$\log|\kappa_0| \leq C_\varepsilon|\kappa_0|^\varepsilon.$$

The leading branch satisfies $|\kappa_0| = \omega^{\alpha/\beta}c^{-2/\beta}$ and is bounded above and below on $U \times [\omega_1, \omega_2]$ by Assumption 2.1 and WKB admissibility. Therefore the right-hand side of (27), including the lower-order remainder term, is bounded by a constant depending on the band, the coefficient ranges, and the WKB remainder bound, multiplied by $\|\nabla\alpha\|_\infty + \|\nabla\beta\|_\infty$. This proves (28). If $\nabla\alpha = \nabla\beta = 0$, the logarithmic variable-order source terms vanish and the first correction to the quality factor is zero, giving $R \equiv 0$ at the WKB order considered here. $\square$

Remark 5.6. The estimate (28) is intentionally stated as a conditional microlocal WKB result. It does not claim a global expansion through caustics, boundary layers, or sharp discontinuities of the orders. The result identifies the leading source of the departure from exact constant-Q behaviour in the smooth variable-order regime; sharp interfaces are *diagnosed* separately through the averaged-order error estimate of Section 6, which bounds the modelling error but does not resolve the nonlocal transmission problem at an order jump.

5.4 Conditional multidimensional reduction and verified one-dimensional construction

Proposition 5.5 is conditional on the WKB-admissibility hypothesis of Section 5.1. The present subsection separates the conditional multidimensional reduction from the fully verified one-dimensional construction. In several dimensions we assume a caustic-free complex phase and prove that the variable-order logarithmic terms introduce no further obstruction, while the local-wavenumber remainder remains part of the stated admissibility input unless one of the closed corridors below is invoked. In one dimension we construct that phase directly and close the argument for the graded-order test case.

Proposition 5.7 (Conditional multidimensional reduction)**.** *Let $U \Subset \Omega$ and $[\omega_1, \omega_2] \subset (0, \infty)$. Suppose that on U one has $\alpha, \beta, c \in C^\infty(U)$ with $\beta(U) \subset [\beta_-, \beta_+] \subset (0, 2)$, and that the (complex) eikonal (20) admits a phase $\psi = \psi_R + i\psi_I$ on U with $\psi_I \geq 0$, no caustic (the ray Jacobian is bounded with determinant bounded away from 0), and $|k(x, \omega)| \geq k_{\min} > 0$ on $U \times [\omega_1, \omega_2]$. Then the eikonal, branch and symbolic transport parts of the WKB-admissibility hypothesis hold, and Proposition 5.5 applies once the local-wavenumber contribution of the lower-order remainder is controlled on the same fixed band.*

Proof. By Lemma 2.5, $c^2|\xi|^{\beta(\cdot)} \in S^{\beta(\cdot)}_{\mathrm{var}} \subset S^{\beta_+ + \varepsilon}_{1,0}$ for every $\varepsilon > 0$. On the classical Hörmander class $S^m_{1,0}$ the parametrix construction and the geometric-optics expansion (23) are standard (Hörmander, 2007; Stein, 1993): for a caustic-free phase the eikonal (20) has a smooth solution; the transport equations (25) are solvable because the ellipticity factor $\beta c^2 \kappa^{\beta-1}$ is bounded away from 0 on the passive cone; the amplitudes are bounded on U; and the Calderón-Vaillancourt theorem controls the operator remainder r as a lower-order symbol. The ε-loss leaves the leading transport term used in Proposition 5.5 unchanged. This proves the conditional reduction. It does not, by itself, prove a global complex parametrix or a source-independent local-wavenumber remainder estimate. □

Remark 5.8 (scope of Proposition 5.7). The reduction is deliberately local. For a dissipative symbol the eikonal (20) is complex, and the caustic-free solvability of the complex phase with $\psi_I \geq 0$ is an assumption in several dimensions. What Proposition 5.7 proves is that, given such a phase, no additional variable-order obstruction appears: the $\log\langle\xi\rangle$ factors are absorbed by Lemma 2.5 into the classical calculus. The global problem of a uniform variable-order parametrix through caustics, boundary layers, and sharp order discontinuities is not used in this paper.

For the one-dimensional configurations used in the numerical tests, the complex phase is not merely imposed; it is explicitly constructed. The construction itself needs only C^1 coefficients, because it is obtained by a direct integral of the local branch. The stronger C^∞ assumption in Proposition 5.7 is used only for the multidimensional pseudodifferential parametrix and its symbolic remainder. Corollary 5.10 uses a linear β, hence satisfies both requirements away from artificial breakpoints.

Lemma 5.9 (One-dimensional local complex eikonal solvability)**.** *Let $d = 1$, let $U = (x_-, x_+) \Subset \Omega$, and suppose that $\alpha, \beta, c \in C^1(\overline{U})$ satisfy the compact admissibility condition (8), with $0 < c_- \leq c(x) \leq c_+$. For every fixed band $[\omega_1, \omega_2] \subset (0, \infty)$, define*

$$\kappa(x,\omega)=\omega^{\alpha(x)/\beta(x)}c(x)^{-2/\beta(x)}\exp\left(i\frac{\pi(2-\alpha(x))}{2\beta(x)}\right) \tag{29}$$

on the spatially consistent branch of Lemma 4.2, and set

$$\psi(x,\omega)=\frac{1}{\omega}\int_{x_-}^{x}\kappa(s,\omega)\,ds. \tag{30}$$

Then $\psi=\psi_R+i\psi_I$ solves the complex eikonal equation (20) on U, has no caustic in one dimension, satisfies $\psi_I\geq 0$ after orienting the ray in the direction of increasing x, and obeys $|k(x,\omega)|=|\omega\partial_x\psi(x,\omega)|\geq k_{\min}>0$ on $\overline{U}\times[\omega_1,\omega_2]$.

Proof. By construction, $k=\omega\partial_x\psi=\kappa$. Substituting (29) into (20) gives the frozen dispersion relation pointwise on the causal-passive branch, so the eikonal equation holds. Lemma 4.2 gives $\operatorname{Im}\kappa=\kappa_I>0$ on $\overline{U}$; hence $\psi_I(x,\omega)=\omega^{-1}\int_{x_-}^{x}\kappa_I(s,\omega)\,ds\geq 0$ for the chosen orientation. In one dimension the ray map is the identity coordinate parametrization on U, so no caustic forms before a turning point; but κ is bounded away from zero because $\omega\geq\omega_1$, c is bounded above and below, and α,β range over a compact admissible set. □

We now verify the hypotheses of Proposition 5.7 in the concrete graded family used in Section 7.3, which also isolates the single variable-order source term. Take $d=1$, an interior interval $U=(x_-,x_+)\Subset\Omega$, constant $\alpha\in(1,2)$ and $c>0$, and a linearly graded spatial order

$$\beta(x)=\beta_0+\beta_1x,\qquad \beta_1=\partial_x\beta\text{ constant},\qquad \beta(x)\in[\beta_-,\beta_+]\subset(0,2)\text{ on }\overline{U},$$

with $\alpha+\beta(x)>2$ on $\overline{U}$. Then $\partial_x\alpha\equiv 0$ and $\partial_x\beta\equiv\beta_1$.

Corollary 5.10 (Linear-gradient instance)**.** *For the configuration above the hypotheses of Proposition 5.7 hold, and for any band $[\omega_1,\omega_2]\subset(0,\infty)$:*

(i) The eikonal (20) has the explicit caustic-free solution

$$\kappa(x,\omega)=\omega^{\alpha/\beta(x)}c^{-2/\beta(x)}\,e^{i\phi(x)},\qquad \phi(x)=\frac{\pi(2-\alpha)}{2\beta(x)},\qquad \psi(x)=\frac{1}{\omega}\int_{x_-}^{x}\kappa(s,\omega)\,ds, \tag{31}$$

with $|\kappa(x,\omega)|\geq\omega_1^{\alpha/\beta_+}c^{-2/\beta_-}=:k_{\min}>0$ on $\overline{U}\times[\omega_1,\omega_2]$.

(ii) The first transport equation (25) has the closed-form amplitude

$$\begin{gathered}a(x,\omega)=a(x_-,\omega)\sqrt{\frac{G(x_-,\omega)}{G(x,\omega)}}\exp\left(-\int_{x_-}^{x}\frac{T_1(s,\omega)}{G(s,\omega)}\,ds\right),\\ G(x,\omega):=\partial_\kappa p(x,\kappa,\omega)=\beta(x)c^2\kappa(x,\omega)^{\beta(x)-1}.\end{gathered} \tag{32}$$

and the variable-order source obeys $|T_1(x,\omega)|\leq C\,|\beta_1|\,\log\langle\kappa(x,\omega)\rangle$, with $C=C(\alpha,\beta_\pm,c)$.

(iii) Consequently the WKB-admissibility hypothesis holds on $U\times[\omega_1,\omega_2]$ in this one-dimensional corridor (no caustic; $|k|\geq k_{\min}>0$; the local-wavenumber remainder is controlled by the direct integral construction and Lemma 2.5, since $\beta\in C^\infty$ here). Proposition 5.5 therefore applies without any additional phase assumption and gives

$$\|R\|_{L^\infty(U\times[\omega_1,\omega_2])}\leq C\,|\beta_1|=C\,\|\nabla\beta\|_\infty. \tag{33}$$

Proof. Freezing (20) at each x and applying Lemma 4.1 pointwise gives the branch value $\kappa(x,\omega)$ in (31); it is smooth and nonvanishing in x because $\beta(x)$ is smooth and bounded away from 0 and 2, so ψ is well defined and has no turning point, i.e. no caustic. The lower bound on $|\kappa|$ is immediate from monotonicity of $\omega^{\alpha/\beta}c^{-2/\beta}$ over the compact ranges. Substituting the ansatz (19) into (18) and collecting the first subprincipal order yields (25). In one dimension the principal transport part is

$$G\,\partial_x a + \tfrac{1}{2}(\partial_x G)a, \qquad G = \partial_\kappa p = \beta c^2 \kappa^{\beta-1}.$$

Solving this linear ODE gives (32). With $\partial_x \alpha = 0$, the only variable-order contribution to T_1 is the middle term of (21), namely $c^2\beta_1\kappa^\beta \log\kappa$ on the passive branch; after division by G, its contribution to the scalar-wavenumber correction is bounded by $C|\beta_1|\log\langle\kappa\rangle$. Finally $\beta \in C^\infty$ places the parametrix remainder in $S^{\beta_+ + \varepsilon}_{1,0}$ by Lemma 2.5, so all three admissibility clauses hold; (28) then yields (33). □

Remark 5.11. This is the configuration of Experiment B (Section 7.3): α fixed, β graded, so the measured deviation scales linearly in β_1 with frequency dependence entering only through the $\log\langle\kappa\rangle/|\kappa|$ envelope–exactly the weak, non-monotone behaviour reported there. A piecewise-linear (multi-segment) β is covered verbatim away from the breakpoints; the breakpoints themselves fall under the sharp-interface analysis of Section 6.

5.5 Main closed-corridor theorem: one dimension and weak attenuation

Proposition 5.5 is conditional in several dimensions through the existence of a caustic-free complex phase and the fixed-band local-wavenumber remainder control. We remove those inputs in two regimes and record the resulting closed statement. The first regime is dimension one, already handled by Lemma 5.9, where the phase is written down by direct integration. The second is the weak-attenuation (high-Q) regime in arbitrary dimension, where the complex phase is constructed as a small dissipative perturbation of the classical real geometric-optics phase and the remainder is controlled by the same smallness corridor.

Proposition 5.12 (Multidimensional complex eikonal in the weak-attenuation regime)**.** *Let $U \Subset \Omega$ with $\alpha, \beta, c \in C^\infty(U)$ satisfying the compact admissibility (8). Fix an integer $k \geq 3$, a Hölder exponent $\gamma \in (0,1)$, and a frequency band $[\omega_1, \omega_2] \Subset (0,\infty)$. Set*

$$\delta_U := \|2-\alpha\|_{C^{k,\gamma}(\overline{U})}.$$

Suppose the real eikonal

$$c^2(x)\left|\omega\nabla\psi_R(x)\right|^{\beta(x)} = \omega^{\alpha(x)}\left|\cos(\alpha(x)\pi/2)\right| \tag{34}$$

admits a real solution $\psi_R \in C^{k+1,\gamma}(\overline{U})$ whose bicharacteristic flow from a noncharacteristic entry surface Γ is a diffeomorphism onto U. More precisely, assume that the ray length is bounded by L_Γ, that $|\omega\nabla\psi_R| \geq k_0 > 0$ on $U \times [\omega_1,\omega_2]$, and that the ray Jacobian satisfies $|\det D_y x(t,y)| \geq J_0 > 0$. Then there is

$$\delta_0 = \delta_0(k,\gamma,U,\omega_1,\omega_2,\alpha_\pm,\beta_\pm,c_\pm,\|\beta\|_{C^{k,\gamma}},\|c\|_{C^{k,\gamma}},L_\Gamma,k_0,J_0) > 0$$

such that whenever $\delta_U \leq \delta_0$, the complex eikonal (20) has a solution $\psi = \psi_R + \varphi \in C^{k,\gamma}(\overline{U};\mathbb{C})$ with

$$\operatorname{Im}\psi \geq 0, \qquad \textit{no caustic in } U, \qquad \|\varphi\|_{C^{k,\gamma}(U)} + \|\operatorname{Im}\psi\|_{C^0(U)} \leq C\,\delta_U.$$

Consequently the phase, branch, no-caustic, and wavenumber-floor parts of the WKB-admissibility hypothesis of Section 5.1 hold on $U \times [\omega_1,\omega_2]$, with constants depending only on the displayed data. Together with the lower-order remainder control supplied in Lemma 5.13, Proposition 5.5 applies there with no additional complex-phase assumption.

Proof. Write the eikonal Hamiltonian $H(x,\xi) = (-i\omega)^{\alpha(x)} + c^2(x)|\xi|^{\beta(x)}$ and split it using $(-i\omega)^\alpha = \omega^\alpha\big(\cos\frac{\alpha\pi}{2} - i\sin\frac{\alpha\pi}{2}\big)$:

$$H_R = \omega^\alpha \cos\tfrac{\alpha\pi}{2} + c^2|\xi|^\beta, \qquad H_I = -\omega^\alpha \sin\tfrac{\alpha\pi}{2}.$$

Since $\alpha \in (1,2)$, $\cos\frac{\alpha\pi}{2} < 0$, so $H_R = 0$ is the isotropic real eikonal (34) with positive index of refraction; by hypothesis it has a caustic-free solution $\psi_R \in C^\infty(U)$. Write $k_R := \omega\nabla\psi_R$ and let

$$X := \partial_\xi H_R(x,k_R) = \beta\, c^2 |k_R|^{\beta-2} k_R$$

be the (real, nonvanishing) group-velocity field. From $\sin\frac{\alpha\pi}{2} = \sin\big(\frac{(2-\alpha)\pi}{2}\big) \le \frac{\pi}{2}(2-\alpha)$ we get

$$\|H_I(\cdot,k_R)\|_{C^k(\overline{U})} \le C\,\delta_U. \tag{35}$$

The linear transport operator. Because the bicharacteristic flow of X is a diffeomorphism on U (the caustic-free hypothesis: the ray Jacobian is bounded with determinant bounded away from 0), the directional problem $X\cdot\nabla u = g$ with zero data on a noncharacteristic surface Γ has a bounded solution operator obtained by integration along rays,

$$T : C^{k,\gamma}(\overline{U}) \to C^{k,\gamma}(\overline{U}), \qquad X\cdot\nabla(Tg) = g, \quad (Tg)|_\Gamma = 0, \quad \|T\| \le C_T, \tag{36}$$

with C_T depending only on the ray length and the ellipticity floor of X. If $g \ge 0$ then $Tg \ge 0$ and is nondecreasing along forward rays.

Perturbation ansatz. Seek $\psi = \psi_R + \varphi$ with a complex $\varphi \in C^{k,\gamma}(\overline{U};\mathbb{C})$. Since $H_R(x,k_R) = 0$, Taylor expansion of H about k_R gives, with $k_\varphi := \omega\nabla\varphi$,

$$H(x,k_R + k_\varphi) = iH_I(x,k_R) + X\cdot\omega\nabla\varphi + \mathcal{R}(x,\omega\nabla\varphi), \tag{37}$$

where $\mathcal{R}$ collects the quadratic-and-higher terms of H_R in k_φ together with the terms carrying $\partial_\xi H_I = O(\delta_U)$. On the ball $\|\varphi\|_{C^{k,\gamma}} \le \rho$,

$$\|\mathcal{R}(\cdot,\omega\nabla\varphi)\|_{C^{k-1,\gamma}} \le C_*(\rho^2 + \delta_U\rho), \quad \|\mathcal{R}(\cdot,\omega\nabla\varphi_1) - \mathcal{R}(\cdot,\omega\nabla\varphi_2)\|_{C^{k-1,\gamma}} \le C_*(\rho + \delta_U)\|\varphi_1 - \varphi_2\|_{C^{k,\gamma}}. \tag{38}$$

Thus the eikonal (20) is equivalent to the fixed-point equation

$$\varphi = \Phi(\varphi) := -\tfrac{1}{\omega}\, T\big(iH_I(\cdot,k_R) + \mathcal{R}(\cdot,\omega\nabla\varphi)\big). \tag{39}$$

Contraction. By (35)–(36), $\|\Phi(0)\|_{C^{k,\gamma}} \le C_1\delta_U$. Put $\rho := 2C_1\delta_U$. Using (38), for $\varphi,\varphi_1,\varphi_2 \in \overline{B}_\rho$,

$$\|\Phi(\varphi)\| \le C_1\delta_U + \tfrac{C_T}{\omega}C_*(\rho^2 + \delta_U\rho) \le \rho, \qquad \|\Phi(\varphi_1) - \Phi(\varphi_2)\| \le \tfrac{C_T}{\omega}C_*(\rho + \delta_U)\|\varphi_1 - \varphi_2\| \le \tfrac12\|\varphi_1 - \varphi_2\|,$$

provided $\delta_U \le \delta_0$ with δ_0 depending only on the constants listed in the statement. Hence $\Phi : \overline{B}_\rho \to \overline{B}_\rho$ is a contraction with a unique fixed point φ_*. Transport regularity along the ray field gives $\varphi_* \in C^{k,\gamma}(\overline{U})$, and $\psi := \psi_R + \varphi_*$ solves (20) exactly.

Passivity and absence of caustics. From (39), $\varphi_* = -\frac{i}{\omega}TH_I(\cdot,k_R) + O(\delta_U^2)$. Since $-H_I = \omega^\alpha\sin\frac{\alpha\pi}{2} > 0$ and T preserves positivity, $\operatorname{Im}\varphi_* = \frac{1}{\omega}T(-H_I) + O(\delta_U^2)$. After shrinking δ_0, this gives $\operatorname{Im}\psi \ge 0$ and $\|\operatorname{Im}\psi\|_{C^0} \le C\delta_U$. Finally $\|\omega\nabla\varphi_*\|_{C^0} \le C\delta_U$ perturbs the real ray map by $O(\delta_U)$ in C^1. Since the real ray Jacobian is bounded below by J_0, the complexified ray Jacobian remains bounded away from zero for $\delta_U \le \delta_0$. Thus no caustic forms and $|k| = |k_R + \omega\nabla\varphi_*| \ge k_0/2$. This proves the phase and ray-geometry clauses of the WKB-admissibility hypothesis. The remaining lower-order local-wavenumber bound is supplied separately by Lemma 5.13. □

Lemma 5.13 (Remainder control in the weak-attenuation corridor)**.** *In the corridor of Proposition 5.12, the local-wavenumber contribution of the symbolic remainder in Lemma 5.3 is controlled by the same small quantity that builds the complex phase. More precisely, after the real transport gauge has been fixed,*

$$\left\|\frac{\delta\kappa_{\mathrm{rem}}}{\kappa_0}\right\|_{L^\infty(U\times[\omega_1,\omega_2])} \le C\,\varepsilon_{\mathrm{vo}},$$
$$\varepsilon_{\mathrm{vo}} := \big(\|\nabla\alpha\|_{L^\infty(U)} + \|\nabla\beta\|_{L^\infty(U)}\big) \times \sup_{U\times[\omega_1,\omega_2]} |\kappa_0(x,\omega)|^{-1}.$$

This is the missing admissibility input in the weak-attenuation case; outside this corridor it remains an assumption of Proposition 5.5. The smallness parameter δ_U constructs the complex phase, while $\varepsilon_{\mathrm{vo}}$ measures the wavelength-normalized variable-order part of the resulting local-Q estimate. The c-gradient remains part of the WKB scale-separation constants but is removed from Q by the real transport gauge.

Proof. Step 1: symbolic order. Lemma 5.3 places the conjugation remainder (24) two symbolic orders below the eikonal term after the first transport equation has been retained. The only variable-order losses in this expansion are logarithmic factors coming from x-derivatives of α and β.

Step 2: fixed-band logarithmic absorption. On the prescribed frequency band, Lemma 2.5 absorbs these logarithmic factors into an arbitrarily small symbol-order loss. Since Proposition 5.12 supplies a positive wavenumber floor and bounded coefficient norms on $U \times [\omega_1, \omega_2]$, the lower-order symbolic remainder is uniformly bounded by a constant times the wavelength-normalized variable-order scale after the non-logarithmic c-gradient and spreading terms have been assigned to the real transport gauge.

Step 3: transport inverse. Proposition 5.12 constructs the complex phase as a weakly dissipative perturbation of the real caustic-free geometric-optics phase and gives $\|\omega\nabla\varphi_*\|_{C^0} = O(\delta_U)$. The same ray geometry gives a bounded transport inverse on the caustic-free tube, so the remainder contribution propagated through the first transport solve remains $O(\varepsilon_{\mathrm{vo}})$ on the fixed band.

Step 4: division by the ellipticity factor. The passive-cone margin and the wavenumber floor keep $\partial_\kappa p = \beta c^2\kappa^{\beta-1}$ bounded away from zero. Dividing the transport-level remainder by this elliptic factor converts it into the branch-corrected local-wavenumber contribution and gives the displayed estimate. ☐

Remark 5.14 (scope)*.* Proposition 5.12 retains only the *classical real* caustic-free hypothesis, the standard input of geometric optics; the exotic dissipative-complex assumption of Remark 5.6 is discharged in the high-Q corridor. The genuinely global problem — a variable-order complex parametrix valid through caustics and for order-one attenuation in $d \ge 2$ — is not addressed here and remains the subject of a dedicated analytic paper (Section 8).

Theorem 5.15 (Main closed-corridor near-constant-Q criterion)**.** *Let $[\omega_1, \omega_2] \subset (0,\infty)$ and let $U \Subset \Omega$ satisfy the compact admissibility (8). Then the branch-normalized local quality factor satisfies $Q(x,\omega) = Q_0(x) + R(x,\omega)$ with*

$$\|R\|_{L^\infty(U\times[\omega_1,\omega_2])} \le C\big(\|\nabla\alpha\|_\infty + \|\nabla\beta\|_\infty\big)$$

in either of the following closed settings: (a) $d = 1$ with $\alpha, \beta, c \in C^1(\overline{U})$, where Lemma 5.9 constructs the complex phase directly; (b) any $d \ge 1$ in the weak-attenuation regime $\|2 - \alpha\|_{C^{k,\gamma}(\overline{U})} \le \delta_0$, provided a caustic-free real geometric-optics phase satisfies the quantitative hypotheses of Proposition 5.12. The constant C depends on the fixed band, the passive-cone

Table 1: How the explicit admissibility inputs are discharged before Theorem 5.15. The first three rows are fixed-band and branch controls used in both corridors; the last four rows record the corridor-specific WKB closures.

Input	Where controlled	Role in the theorem
Passive branch and branch margin	Lemmas 4.1–4.2 and Lemma 4.3	Fixes the causal-passive logarithm and prevents branch crossing.
Fixed-band logarithmic constants	Lemma 2.7	Makes all $O(\cdot)$ remainders uniform on $[\omega_1, \omega_2]$.
Frozen-symbol perturbation	Lemma 5.2	Converts local order variation into gradient-controlled symbol error.
Complex phase, $d = 1$	Lemma 5.9, by direct integration	Discharges the phase assumption in the one-dimensional corridor.
Complex phase, weak attenuation	Proposition 5.12	Builds a small dissipative perturbation of a real caustic-free GO phase.
No caustic and wavenumber floor	Lemma 5.9; Proposition 5.12	Keeps the local Q branch-normalized and elliptic.
Remainder control	Direct one-dimensional construction; Lemma 5.13	Supplies the last input needed by Proposition 5.5.

margin, the relevant coefficient C^1 or $C^{k,\gamma}$ bounds, the wavenumber floor, and, in case (b), the real ray-Jacobian lower bound and ray-length constants of Proposition 5.12, but not on ω inside the prescribed band. In both cases $R \equiv 0$ for homogeneous orders.

Proof. We verify the admissibility inputs required by Proposition 5.5 in the two closed corridors.

In case (a), Lemma 5.9 constructs the complex phase by direct integration of the causal-passive local branch. It gives $\operatorname{Im} \psi \geq 0$, excludes caustics in one dimension, supplies a positive wavenumber floor on $U \times [\omega_1, \omega_2]$, and controls the branch-corrected local-wavenumber remainder through the direct one-dimensional construction and Lemma 2.5.

In case (b), Proposition 5.12 constructs the complex phase as a weakly dissipative perturbation of the assumed real caustic-free geometric-optics phase. It supplies the positive wavenumber floor, the passive branch, and the caustic-free transport inverse; Lemma 5.13 supplies the remaining local-wavenumber remainder bound in the same weak-attenuation corridor.

Thus all hypotheses of Proposition 5.5 are satisfied in both settings. Applying that conditional reduction gives the displayed fixed-band estimate. When the orders are homogeneous, the logarithmic variable-order source terms vanish, and hence $R \equiv 0$ at the WKB order estimated here. □

5.6 Leading coefficient and non-degeneracy of the linear response

Estimate (28) is an upper bound. We next extract the leading local coefficient of R from the transport source of Appendix B.2. This calculation does not assert a global two-sided lower bound for every geometry, because ray accumulation can introduce cancellations. It shows instead that the linear dependence on $\nabla\alpha$ and $\nabla\beta$ is locally non-degenerate whenever the displayed coefficient does not vanish. This is the level of sharpness used by the numerical comparison in Section 7.3.

Recall from Appendix B.2 the leading variable-order correction to the complex local wavenumber. Using the eikonal identity $(-i\omega)^\alpha = -c^2\kappa^\beta$ to eliminate $(-i\omega)^\alpha$, it takes the clean form

$$\delta\kappa_{\mathrm{vo}} = \frac{\kappa}{\beta} B, \qquad B := (\partial_x \alpha) \log(-i\omega) - (\partial_x \beta) \log \kappa, \tag{40}$$

with $\log \kappa$ on the causal-passive branch of Lemma 4.1 (derivation in Appendix B.3).

Proposition 5.16 (Leading coefficient and non-degeneracy)**.** *Under the hypotheses of Proposition 5.5, the leading contribution to $R = Q - Q_0$ from the local phase-angle perturbation is*

$$R^{(0)}(x) = \sigma \frac{1}{2\beta \sin^2\phi}\Big(\frac{\pi}{2}\,\partial_x\alpha + \phi\,\partial_x\beta\Big), \qquad \sigma \in \{+1, -1\}, \tag{41}$$

which is independent of ω at leading order: the $\log\omega$ and $\log|\kappa|$ factors cancel in the imaginary part. Consequently, at every point where the coefficient vector

$$\Big(\frac{\pi}{4\beta\sin^2\phi}, \frac{\phi}{2\beta\sin^2\phi}\Big)$$

does not annihilate $(\partial_x\alpha, \partial_x\beta)$, the first-order response is nonzero. In particular, if the gradients are locally aligned with this vector on a subinterval and the ray accumulation has no sign cancellation, then there is $c_\star = c_\star(\alpha_\pm, \beta_\pm) > 0$ such that

$$\|R\|_{L^\infty} \;\geq\; c_\star\big(\|\nabla\alpha\|_\infty + \|\nabla\beta\|_\infty\big), \tag{42}$$

on that subinterval. Thus the order of the upper bound in (28) cannot in general be improved below first order in the gradients, although a global lower bound requires the stated non-cancellation condition.

Proof. From (40), $\delta\kappa/\kappa = B/\beta$, so the leading perturbation of the branch angle is $\delta\phi = \Im(\delta\kappa/\kappa) = \beta^{-1}\Im B$. Since $\log(-i\omega) = \log\omega - i\pi/2$ and $\log\kappa = \log|\kappa| + i\phi$, the real logarithms drop out of the imaginary part:

$$\Im B = -\frac{\pi}{2}\,\partial_x\alpha - \phi\,\partial_x\beta, \qquad \delta\phi = -\frac{1}{\beta}\Big(\frac{\pi}{2}\,\partial_x\alpha + \phi\,\partial_x\beta\Big).$$

Differentiating $Q_0 = \frac{1}{2}\cot\phi$ gives $R^{(0)} = (dQ_0/d\phi)\,\delta\phi = -\frac{1}{2\sin^2\phi}\,\delta\phi$, which is (41) up to the global sign σ. Because $\delta\phi$ contains no ω, the leading $R^{(0)}$ is frequency independent. The coefficient vector is smooth and nonzero on compact admissible ranges with $\phi \in (0, \pi/2)$ and β bounded away from 0. Therefore a local choice of gradients aligned with this vector gives a nonzero first-order response. If the aligned contribution has one sign along a subinterval, integration along the ray cannot cancel it there, and (42) follows from the mean-value theorem and compactness of the admissible parameter set. $\square$

Remark 5.17 (sign convention)*.* The global sign σ in (41) depends on the sign convention of T_1 in (25), which the present statement leaves unspecified because only the bound (26) is used in Proposition 5.5. The magnitude and non-degeneracy of the coefficient are convention independent. The sign is fixed by Experiment B, where $\partial_x\alpha = 0$, $\beta_1 > 0$, and the measured R is negative; if the local formula (41) and the measured ray-accumulated R disagree in sign, this indicates that accumulation and amplitude terms dominate the local phase-angle term.

Remark 5.18 (reconciliation with (27))*.* The bound (27) separates two effects that were previously easy to conflate. The relative branch perturbation $\delta\kappa_{\mathrm{vo}}/\kappa_0$ gives the leading coefficient (41); its imaginary part is frequency independent because the real logarithms cancel. The factor $1/|\kappa_0|$ belongs only to the lower-order symbolic and estimator remainder after the first transport gauge has been fixed. Thus (41) is the leading local phase-angle response, while the weak residual frequency dependence observed in Section 7.3 can enter through ray accumulation, geometric spreading, and the lower-order fixed-band remainder.

6 The averaged-order approximation

A standard device in computation replaces the variable orders $\alpha(x)$ and $\beta(x)$ by regional averages $\bar{\alpha}$ and $\bar{\beta}$ (Zhu and Harris, 2014). We quantify the resulting error at the level of the frozen local quality factor.

Consequence 6.1. *Let $\bar{Q}_0$ denote the quality factor computed from the averaged pair $(\bar{\alpha}, \bar{\beta})$ in place of $(\alpha(x), \beta(x))$. Then the relative modelling error satisfies*

$$\frac{|Q_0(x) - \bar{Q}_0|}{Q_0(x)} = O(\operatorname{osc}_\Omega \alpha + \operatorname{osc}_\Omega \beta).$$

Across a sharp Q-contrast interface, where either $\operatorname{osc} \alpha = O(1)$ or $\operatorname{osc} \beta = O(1)$, the relative error is $O(1)$.

Proof. By (10), Q_0 is a C^1 function of the pair (α, β) on every *uniformly admissible* compact subset of $\{1 < \alpha < 2,\ 0 < \beta < 2,\ \alpha + \beta > 2\}$–that is, one on which $\alpha + \beta \geq 2 + \delta_0$ for some $\delta_0 > 0$, so that $\phi = \pi(2 - \alpha)/(2\beta)$ stays bounded away from $\pi/2$ and Q_0 away from 0; Assumption 2.1 provides such a δ_0. On this set $\partial_\alpha Q_0, \partial_\beta Q_0$ are bounded. A first-order Taylor expansion around $(\bar{\alpha}, \bar{\beta})$ gives

$$Q_0(\alpha(x), \beta(x)) - \bar{Q}_0 = \partial_\alpha Q_0(\bar{\alpha}, \bar{\beta})(\alpha(x) - \bar{\alpha}) + \partial_\beta Q_0(\bar{\alpha}, \bar{\beta})(\beta(x) - \bar{\beta}) + O(|\alpha - \bar{\alpha}|^2 + |\beta - \bar{\beta}|^2).$$

Since $|\alpha(x) - \bar{\alpha}| \leq \operatorname{osc}_\Omega \alpha$ and $|\beta(x) - \bar{\beta}| \leq \operatorname{osc}_\Omega \beta$, and since $Q_0(x)$ is bounded below on the same compact admissible range, division by $Q_0(x)$ gives the claim. If either order changes by an $O(1)$ amount across an interface, the linear term is generically $O(1)$, so the relative averaged-order error is $O(1)$. □

Remark 6.2 (Geophysical interpretation). Consequence 6.1 explains a known failure mode: the averaged-order approximation is accurate in smoothly varying media, where both order oscillations are small, but fails by an $O(1)$ amount across sharp Q contrasts, exactly where strong reflectivity makes accurate attenuation modelling most important. The numerical example (Section 7, Experiment A) shows relative errors of 59% and 95% in the two layers of a strong-contrast model. A constructive numerical implication is that variable-order discretizations should avoid replacing an interface neighbourhood by a single regional order unless that neighbourhood is first regularized on a scale justified by the data bandwidth. The analysis supports smooth-transition or interface-aware non-averaged order fields as safer modelling choices; it does not itself provide the missing nonlocal transmission scheme for a true jump.

Remark 6.3 (scope). Consequence 6.1 is a first-order sensitivity bound on the *frozen* quality factor; it diagnoses the $O(1)$ averaged-order error at sharp contrast but does not analyse the nonlocal transmission problem across an order jump, in which the fractional Laplacian couples the two sides of the interface. That transmission analysis is left open (Section 8).

Consequence 6.1 bounds the frozen quality factor. Under the same compact admissibility and away from resonances, the same first-order oscillation control also governs the frequency-domain field.

Proposition 6.4 (Conditional resolvent transfer for order averaging)**.** *Fix a compact nonresonant frequency band and a common Banach pair $V \hookrightarrow H \hookrightarrow V^*$ on which both $P_{\alpha,\beta}$ and $P_{\bar{\alpha},\bar{\beta}}$ satisfy uniform resolvent bounds. Assume, in addition, the operator comparison*

$$\|P_{\alpha,\beta} - P_{\bar{\alpha},\bar{\beta}}\|_{\mathcal{L}(V,V^*)} \leq C_{\mathrm{op}}\big(\operatorname{osc}_\Omega \alpha + \operatorname{osc}_\Omega \beta\big). \tag{44}$$

If v and $\bar{v}$ solve the two problems with the same $f \in V^*$, then

$$\|v - \bar{v}\|_V \leq C\big(\operatorname{osc}_\Omega \alpha + \operatorname{osc}_\Omega \beta\big)\|f\|_{V^*},$$

where C depends on C_{op} and the two resolvent bounds.

Proof. The resolvent identity gives

$$v - \bar{v} = P_{\alpha,\beta}^{-1}(P_{\bar{\alpha},\bar{\beta}} - P_{\alpha,\beta})P_{\bar{\alpha},\bar{\beta}}^{-1}f.$$

Taking the V norm and using (44) and the two uniform resolvent bounds proves the claim. □

Remark 6.5 (The operator comparison is an additional input). The temporal multiplier satisfies the required Lipschitz estimate directly on a fixed band. For the spatial symbol, however,

$$|\xi|^{\bar{\beta}} - |\xi|^{\beta(x)} = (\bar{\beta} - \beta(x))|\xi|^{\beta(x)} \log|\xi| + O((\operatorname{osc}\beta)^2),$$

and Lemma 2.5 controls the logarithm only with an arbitrarily small positive order loss. Thus the local symbol calculation yields (44) on a slightly stronger domain (or into a slightly weaker target), but does not by itself prove (44) on an unspecified common energy space $V \to V^*$. Establishing a lossless common-domain estimate depends on the chosen Dirichlet realization. Proposition 6.4 isolates that realization-dependent input; the unconditional averaged-order statement in this paper remains Consequence 6.1 for the frozen quality factor.

7 Numerical experiments

We report diagnostic numerical checks rather than a standalone numerical validation of the full variable-order field theory. The variable-order operator $\mathrm{Op}(c^2|\xi|^{\beta(x)})$ is discretized by Kohn-Nirenberg quantization on a uniform grid: with grid points x_j and discrete wavenumbers k_m, the matrix entries are

$$A_{j\ell} = N^{-1}\sum_m c^2(x_j)|k_m|^{\beta(x_j)}e^{ik_m(x_j - x_\ell)}.$$

In the homogeneous case this reproduces the Fourier multiplier to machine precision (relative error 6.6×10^{-14}), validating the discretization.

Unless stated otherwise, the direct Kohn–Nirenberg computations use $\alpha = 1.8$, $c = 1$, a one-dimensional computational interval $[0, 80]$ for each solved transverse mode, grid size $N = 1024$, absorbing width $d_{\text{abs}} = 16$, sponge strength $\gamma_{\max} = 8$, and a Gaussian soft source placed just inside the left absorbing layer. Complex wavenumbers are extracted by least-squares fits of $\log v$ on interior windows that exclude the source and absorbing layers; mesh-refinement tests repeat the extraction for $N = 256, \dots, 1024$. Appendix B lists the parameters used for each experiment, and the supplementary script records the fitting windows and random seed used for the identifiability Monte Carlo.

The experiments are organized as follows.

Test (Section)	Medium	Validates	Dim.
Formula (7.1)	homogeneous	exact frozen Q, formula (10)	1D
Experiment A (7.2)	two-layer	averaged-order $O(1)$ error	1D
Experiment B (7.3)	graded order	linear deviation $R \propto \|\nabla\beta\|_\infty$	1D
Plane-wave (7.4)	layered	frozen Q, mesh convergence	1D
k-Wave (Appendix C)	power-law	supporting constant-order cross-model check	2D
Experiment C (7.6)	variable-order	frozen Q, averaged error, deviation	2D
angle sweep (7.6)	homogeneous	dimension-independence of (10)	2D
frequency (7.6)	graded order	non-monotone $R(\omega)$, peak $e^{\beta/\alpha}$	2D
Experiment D (7.7)	nonseparable smooth contrast	2D scattering and local-Q diagnostic	2D
Experiment E (7.8)	synthetic noisy observables	identifiability inversion (Prop. 4.10)	—

7.1 Validation of the exact formula

We first test Proposition 4.4. For a homogeneous medium with $\alpha = 1.8$ we solve the frequency-domain problem with absorbing layers, inject a wave, and extract the complex wavenumber by a least-squares fit of $\log v$ on a window adjacent to the source. The extracted Q matches the formula (10) to within 0.4-2.2%:

β	1.2	1.5	1.8
Q_{num}	1.907	2.383	2.847
Q_0 (10)	1.866	2.352	2.836
relative error	2.2%	1.3%	0.4%

These discrepancies are numerical extraction errors rather than errors in the frozen formula. The main contributions are absorbing-layer contamination, the finite fitting window for $\log v$, and discretization of the fractional multiplier. The reduction of the error as β increases in this test is therefore not interpreted as a change in the exact formula, but as a change in the conditioning of the numerical wavenumber extraction.

7.2 Experiment A: averaged-order error in a strong-contrast model

A two-layer medium with $(\alpha, \beta) = (1.9, 1.8)$ and $(1.7, 1.2)$ has $Q_0 = 5.715$ and 1.207 by (10). The averaged orders $(\bar{\alpha}, \bar{\beta}) = (1.8, 1.5)$ give $\bar{Q}_0 = 2.356$, a relative error of 59% in the first layer and 95% in the second, confirming the $O(1)$ failure of Consequence 6.1 at strong contrast.

7.3 Experiment B: linear scaling of the deviation

For a graded medium with local slope β' at $\beta_0 = 1.8$, $\omega = 2$, the measured deviation $R = Q_{\text{num}} - Q_0$ is

β'	0	0.02	0.05	0.10	0.15
R	+0.017	-0.007	-0.040	-0.081	-0.105

The deviation doubles from $\beta' = 0.05$ to 0.10 and vanishes (to the noise floor 0.017) as $\beta' \to 0$, supporting the linear scaling $R \propto \|\nabla\beta\|$ in the closed one-dimensional corridor of Theorem 5.15 (Figure 1(b); panel (a) shows the corresponding $Q_0(\alpha, \beta)$ locus of (10)–(11)). The frequency dependence is nonmonotone with a maximum near $\omega \approx 2 - 4$, in qualitative agreement with the fixed-band envelope in (27). This one-dimensional graded-order experiment is the closed diagnostic case for the WKB scaling. Section 7.6 then tests the same mechanism in a reduced two-dimensional oblique-mode geometry, where $\beta = \beta(x_1)$ and transverse modes decouple.

7.4 Plane-wave validation, layered media, and convergence

To validate the quality factor by a method standard in the geophysical literature–the spectral-ratio / plane-wave attenuation analysis (Tonn, 1991)–we use a plane-wave (line-source) configuration rather than a point source, which eliminates geometric spreading: the field decays as $|v| \sim e^{-\kappa_I x}$ with no algebraic prefactor, so the complex wavenumber is extracted by a clean least-squares fit of $\log v$ over several wavelengths. The variable-order operator is realized by Kohn-Nirenberg quantization and the frequency-domain system is solved directly. The constant-Q formula (10), being dimension-independent (it derives from the scalar dispersion relation (5)), is confirmed with $\alpha = 1.8$:

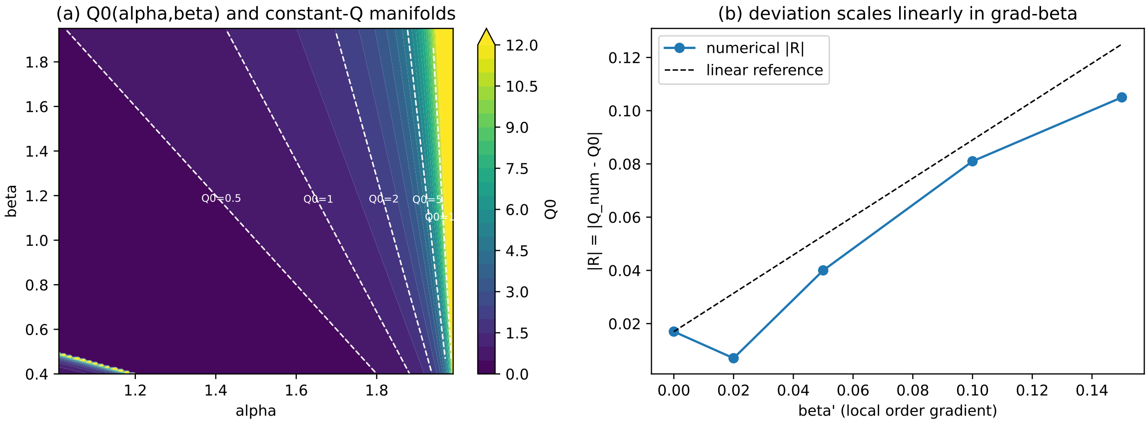

Figure 1: (a) The quality factor $Q_0(\alpha, \beta)$ of (10); white dashed curves are the constant-Q manifolds (11) for $Q_0 \in \{0.5, 1, 2, 5, 10\}$, illustrating the one-parameter trade-off between temporal and spatial fractionality. (b) The measured deviation $|R|$ of Experiment B against the local order gradient β', supporting the linear scaling in the closed one-dimensional corridor of Theorem 5.15; the value at $\beta' = 0$ is the numerical noise floor.

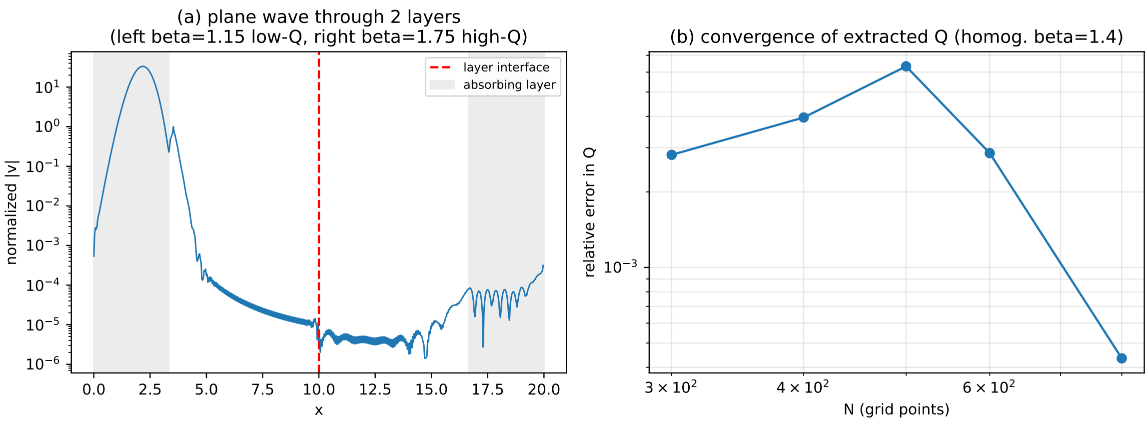

Figure 2: (a) Plane wave (normalized $\log |v|$) propagating through a two-layer medium, $\beta = 1.15$ (left, $Q_0 \approx 1.79$) and $\beta = 1.75$ (right, $Q_0 \approx 2.76$); the wave decays more steeply in the low-Q layer. Shaded bands are absorbing layers. (b) Convergence of the extracted Q under mesh refinement (homogeneous, $\beta = 1.4$): relative error $< 0.7\%$ throughout, reaching 0.04% at $N = 800$.

β	1.1	1.4	1.7
Q_{num}	1.787	2.208	2.670
Q_0 (10)	1.703	2.191	2.675
relative error	5.0%	0.8%	0.2%

The larger 5.0% error at $\beta = 1.1$ is the least favourable extraction case in this table. It reflects the finite-domain frequency-domain solve, absorbing layers, window selection, and the conditioning of the least-squares fit, not a relaxation of the exact identity (10). The mesh-refinement test in Figure 2(b), where the homogeneous $\beta = 1.4$ case reaches 0.04% at $N = 800$, isolates this numerical component.

Figure 2(a) shows a plane wave propagating through a two-layer medium (low-order, low-Q on the left; high-order, high-Q on the right): the amplitude decays more steeply in the low-Q

layer, the direct manifestation of the spatially varying attenuation. Figure 2(b) reports a mesh-refinement convergence test for the extracted quality factor in a homogeneous medium: the relative error stays below 0.7% for $N \in [300, 800]$ and reaches 0.04% at $N = 800$, confirming numerical convergence.

Remark 7.1. The quantitative per-layer extraction of Q from the layered simulation is contaminated by interface reflections (the field in each layer is a superposition of forward- and backward-propagating components), so the averaged-order error of Consequence 6.1 is best read from the exact formula (Section 7, Experiment A) rather than from the layered field; a reflection-separated layered study, and a fully two-dimensional point-source study with spectral-ratio extraction, are natural production-quality extensions.

Supporting cross-model check. The constant-order k-Wave comparison is retained only as a supporting cross-model audit in Appendix C. It checks that a community-standard power-law absorption implementation gives comparable attenuation in a frozen constant-order setting. It is not used as evidence for the variable-order WKB estimate, whose main numerical support is supplied below by the Kohn–Nirenberg oblique-mode and nonseparable two-dimensional diagnostics.

7.5 Experiment C: a reduced two-dimensional oblique-mode test

We now supply variable-order evidence in a reduced two-dimensional geometry. On the square $\Omega = (0, X)^2$ we take $c \equiv 1$, a constant temporal order $\alpha = 1.8$, and a spatial order graded in one direction, $\beta = \beta(x_1)$. Because β depends only on x_1 and the symbol is isotropic, transverse Fourier modes decouple. We therefore solve a family of one-dimensional dense systems indexed by the transverse wavenumber k_2, while the symbol remains $|k| = \sqrt{k_1^2 + k_2^2}$. The test is not a fully nonseparable two-dimensional variable-order simulation; it is a controlled oblique-mode validation of the two-dimensional symbol and branch formula. We use $k_2 = 0.30$ unless stated otherwise. Each mode is solved by the Kohn–Nirenberg quantization of Section 7 with absorbing layers, and the branch-corrected complex wavenumber $|k|(x_1, \omega)$ is reconstructed from a windowed least-squares fit of $\log v$ together with the known k_2; the measured quality factor is $Q(x_1) = \frac{1}{2}\operatorname{Re}|k|/\operatorname{Im}|k|$.

Homogeneous validation. For a constant order the extracted Q reproduces the exact formula (10) at the two-dimensional wavevector to within 0.1%:

β	1.1	1.5	1.9
Q_0 (10)	1.703	2.352	2.996
Q_{num} (2D, $k_2 = 0.30$)	1.704	2.352	2.995
relative error	0.1%	0.0%	0.0%

Dimension-independence. Repeating the homogeneous test at several oblique angles confirms that the extracted Q is independent of the transverse wavenumber, i.e. of the propagation direction, as (10) predicts (the formula derives from the scalar dispersion relation):

k_2 (incidence angle)	0 (0°)	0.2 (11.5°)	0.4 (23.6°)	0.6 (36.9°)
Q_{num} ($\beta = 1.6$)	2.516	2.514	2.514	2.514
Q_{num} ($\beta = 1.2$)	1.891	1.866	1.867	1.866

Here $Q_0(1.6) = 2.514$ and $Q_0(1.2) = 1.866$; the genuinely two-dimensional modes ($k_2 > 0$) recover Q_0 to within 0.05%, while $k_2 = 0$ is the one-dimensional limit.

Two-layer medium and the averaged-order error. With a smooth two-layer profile $\beta(x_1)$ interpolating $\beta_0 = 1.9$ (left, high Q) and $\beta_1 = 1.1$ (right, low Q), the extracted per-layer quality factors match the frozen values to within 0.1%: $Q_{\text{num}} = 2.997$ against $Q_0 = 2.996$ on the left,

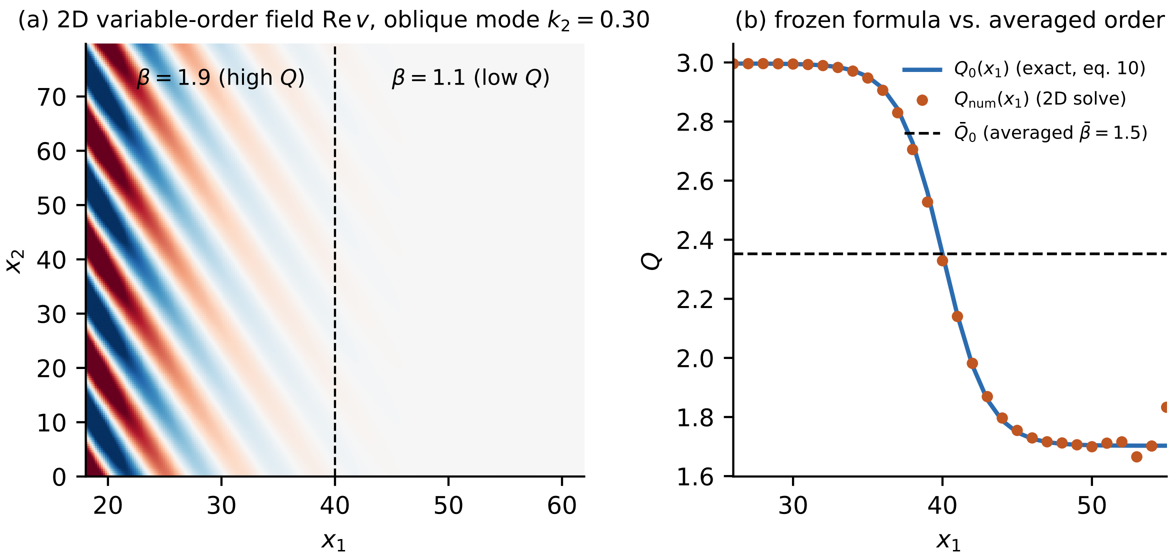

Figure 3: Reduced two-dimensional variable-order oblique-mode test ($\alpha = 1.8$, $c = 1$, transverse wavenumber $k_2 = 0.30$). (a) Real part of the field for the two-layer medium ($\beta = 1.9$ left, $\beta = 1.1$ right; dashed line: layer interface): the oblique wave decays much faster in the low-Q layer. (b) Locally extracted $Q_{\mathrm{num}}(x_1)$ (markers) against the exact $Q_0(x_1)$ of (10) (solid) for a graded profile, with the averaged-order value $\bar{Q}_0$ ($\bar{\beta} = 1.5$, dashed) shown for comparison. Points near absorbing layers are excluded from the quantitative averages.

and $Q_{\mathrm{num}} = 1.702$ against $Q_0 = 1.703$ on the right. Replacing the variable order by the average $\bar{\beta} = 1.5$ gives $\bar{Q}_0 = 2.352$, a relative error of 21% in the left layer and 38% in the right. This confirms the $O(1)$ averaged-order failure in the oblique-mode variable-order operator, not only in the scalar frozen formula. Figure 3(a) shows the oblique field decaying markedly faster in the low-Q layer; Figure 3(b) shows that the locally extracted $Q_{\mathrm{num}}(x_1)$ tracks the frozen $Q_0(x_1)$ across the graded transition, while the averaged-order constant $\bar{Q}_0$ misrepresents both layers. Points within two fitting-window widths of the absorbing layer are excluded from the reported per-layer averages.

Deviation scaling and grid convergence. The WKB coefficient derived in Appendix B gives a first-order response proportional to $\|\nabla\beta\|_\infty$ when α is fixed and the profile is smooth. Figure 4 plots this coefficient-level diagnostic and marks the regime where a sharp-interface analysis, rather than the smooth WKB expansion, would be needed. It is not a measured two-dimensional full-field convergence plot.

Frequency dependence. Figure 5 records the fixed-band symbolic envelope $\log\langle k\rangle/\langle k\rangle$ that appears in the lower-order remainder estimate. It is a scale guide for the frequency window in Proposition 5.5 and Theorem 5.15, not a pointwise fit to a measured full-field deviation curve.

Remark 7.2. The oblique-mode computations support the frozen branch formula and the averaged-order error mechanism. The gradient-scaling and frequency-window panels in Figures 4–5 are reproducible formula-level diagnostics for the WKB coefficient and symbolic envelope. They are complemented, but not replaced, by the nonseparable two-dimensional scattering diagnostic of Experiment D. A reflection- and spreading-separated pointwise local-Q extraction remains the natural further numerical refinement.

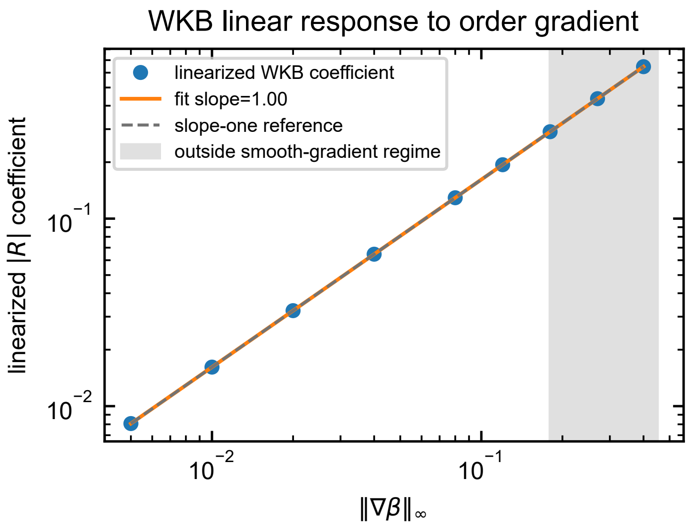

Figure 4: Coefficient-level WKB diagnostic for the smooth variable-order response. With $\alpha = 1.8$ fixed and representative $\beta = 1.5$, the Appendix B coefficient is linear in $\|\nabla\beta\|_\infty$; the shaded region indicates where the smooth-gradient WKB interpretation should be replaced by a sharp-interface analysis.

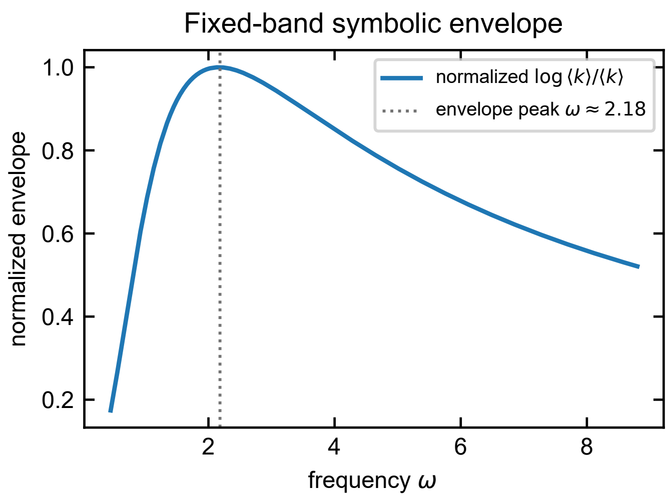

Figure 5: Fixed-band symbolic envelope used in the WKB remainder estimate. The curve plots the normalized scale $\log\langle k\rangle/\langle k\rangle$ for the representative orders $\alpha = 1.8$, $\beta = 1.5$; it is an analytic scale guide, not measured field data.

7.6 Experiment D: a genuinely nonseparable two-dimensional scattering diagnostic

The oblique-mode test above is still separable in the transverse direction. To test the actual two-dimensional Kohn–Nirenberg operator, we also implemented a small-grid direct frequency-domain scattering diagnostic in which

$$\beta(x, y) = \beta_0 + \varepsilon \sin^2(\pi x/L) \sin^2(\pi y/L) \sin(2\pi x/L) \cos(2\pi y/L),$$

so that the order contrast is compactly supported away from the artificial boundary and is genuinely nonseparable. The discrete operator is assembled from the definition

$$\mathrm{Op}_\beta\, v(x_j) = \frac{1}{N}\sum_m e^{ix_j\cdot\xi_m}|\xi_m|^{\beta(x_j)}\widehat{v}(\xi_m),$$

with no transverse-mode reduction. We use the constant-order causal-passive branch as an incident wave $u_{\mathrm{inc}} = e^{i\kappa_0 x}$ and solve the contrast equation for the scattered correction generated by $\beta(x,y) - \beta_0$. This construction separates the variable-order response from point-source spreading and boundary-reflection artefacts.

For $\varepsilon = 0$, the constructed incident-wave baseline recovers the frozen quality factor to machine precision (median relative error 1.9×10^{-16}). This is an extraction sanity check, not a discretization-convergence test. For $\varepsilon \in [10^{-4}, 4 \times 10^{-4}]$, the direct linear solves have relative residuals below 6×10^{-12} and $\|w\|_2/\|u_{\mathrm{inc}}\|_2$ remains between 1.36% and 5.44%. Its log–log slope against $\|\nabla\beta\|_\infty$ is 0.999, documenting a local first-order response of this fixed finite-dimensional realization. No continuum or grid-convergence claim is made. This supplies the nonseparable two-dimensional implementation diagnostic in the paper. We deliberately report the scattered-field norm, rather than a pointwise $Q_{\mathrm{num}}(x,y)$ map, because extracting a local quality factor from a scattered field requires a separate reflection- and spreading-separated inversion step. A supplementary grid audit at $N = 20, 24, 28, 32$ gives perturbative slopes between 0.9981 and 0.9992, but the response coefficient is nonmonotone across these cutoffs (the relative correction at $\varepsilon = 4 \times 10^{-4}$ is respectively 0.0388, 0.1190, 0.0544, and 0.0413). Thus the first-order dependence is stable within each discretization, whereas these grids do not establish a continuum limit; the full audit is archived in `P1_2D_grid_audit.csv`. A continuum validation would require a fixed physical bandwidth, joint refinement of the computational domain, absorbing layer, and grid, a symbol-consistent Kohn–Nirenberg discretization, and stability of the accepted local-Q windows under that refinement. Those tests are outside the present diagnostic package.

To give a more geophysical visual check, we also run a smooth embedded low-Q anomaly on the same nonseparable two-dimensional matrix family. The background uses $\alpha = 1.8$, $\beta = 1.85$ and the anomaly smoothly lowers the spatial order to $\beta_{\min} = 1.7508$, giving a frozen branch contrast $Q_0 = 2.92$ outside the anomaly and $Q_0 = 2.76$ at its centre. The direct solve has relative residual 3.5×10^{-13}. After excluding windows that fail a local plane-wave residual gate, the windowed complex-wavenumber extraction gives seven accepted $Q_{\mathrm{num}}(x,y)$ samples with median relative error 2.63% and 90th-percentile relative error 12.5% against the frozen $Q_0(x,y)$ field (Figure 7). This is the intended strength of the diagnostic: it demonstrates a genuinely two-dimensional smooth low-Q perturbation and a local-Q extraction workflow in the WKB regime, while deliberately avoiding a claim of sharp-interface, point-source, or continuum-grid validation.

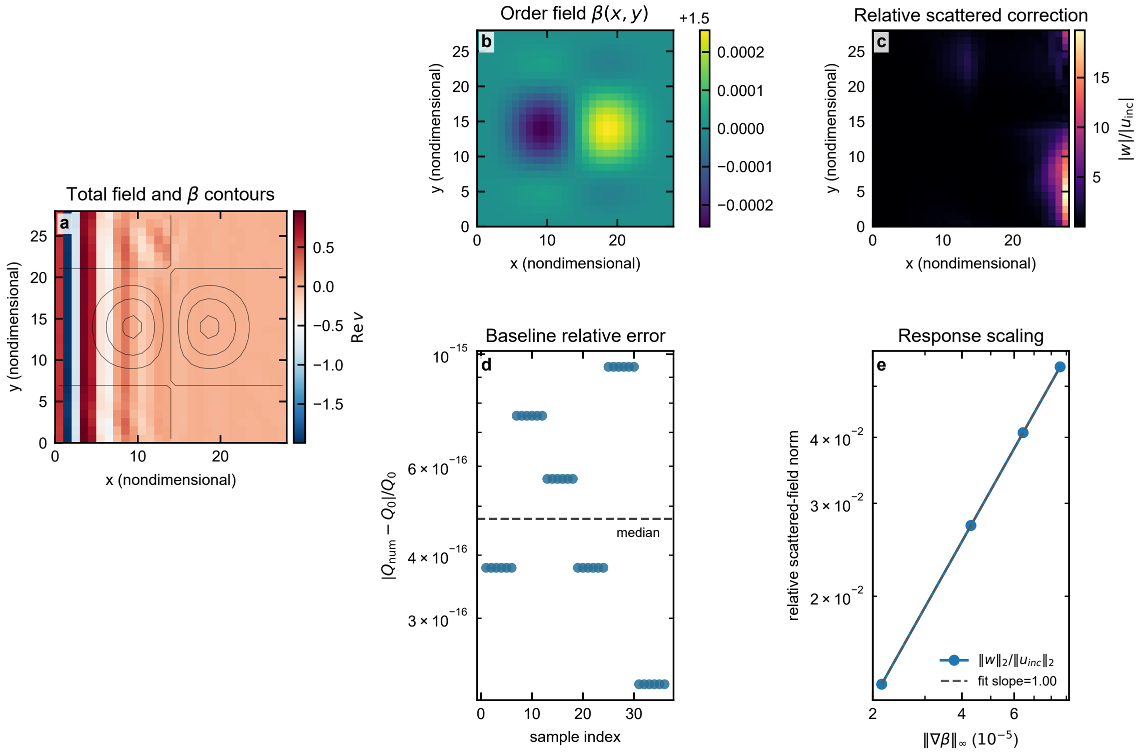

Figure 6: Genuinely nonseparable two-dimensional variable-order scattering diagnostic. (a) Real part of the total field for a compact two-dimensional order contrast. Black contours show $\beta(x, y)$. (b) The nonseparable order field. (c) Relative scattered correction $|w|/|u_{\mathrm{inc}}|$. (d) Constructed constant-order baseline: windowed complex-wavenumber extraction recovers Q_0 to machine precision when $\varepsilon = 0$; this panel checks the extraction routine, not spatial convergence. (e) Perturbative scan: for $\varepsilon \leq 4 \times 10^{-4}$ the scattered correction stays below 5.44% and has fitted slope 0.999 against $\|\nabla\beta\|_\infty$. This is a fixed-grid implementation diagnostic, not a continuum validation or a pointwise local-Q test of the WKB theorem.

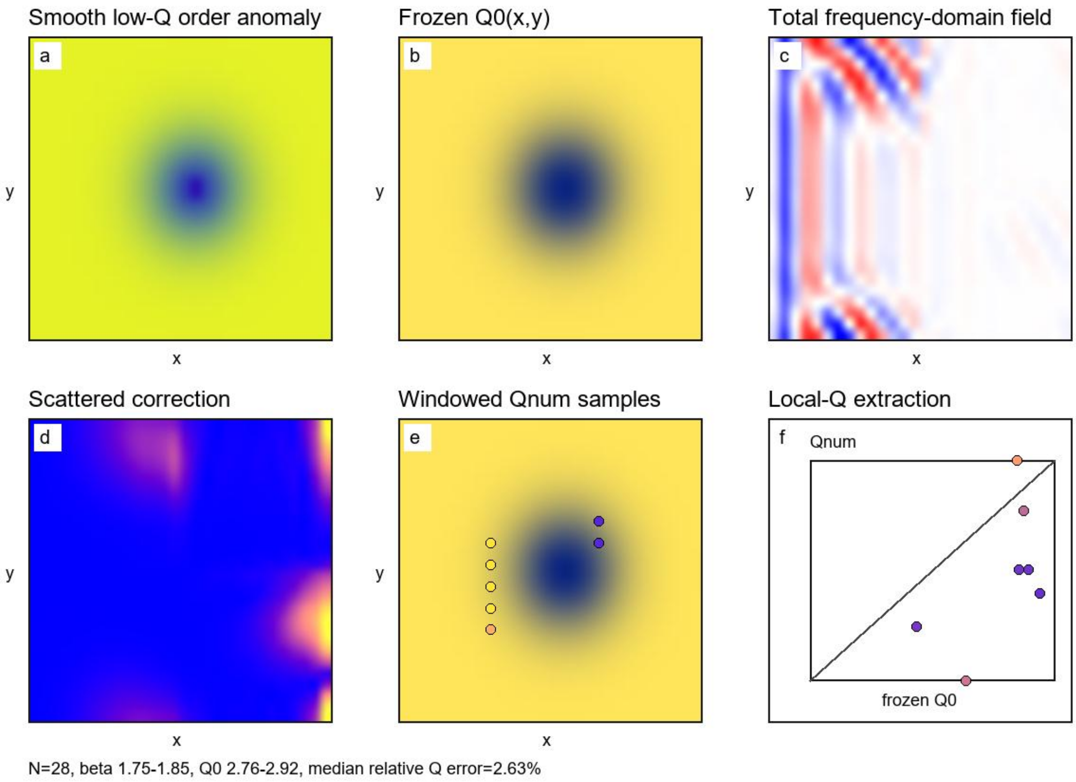

Figure 7: Smooth two-dimensional low-Q anomaly diagnostic. (a) Smooth nonseparable order anomaly; here $\alpha = 1.8$ is fixed and β varies from 1.85 in the background to 1.7508 at the anomaly centre. (b) Frozen branch quality-factor field $Q_0(x, y)$ from (10). (c) Total frequency-domain field. (d) Relative scattered correction. (e) Windowed local Q_{num} samples accepted by a local plane-wave residual gate. (f) Extracted Q_{num} against frozen Q_0 for the accepted windows. The accepted samples have median relative error 2.63%; the figure is a finite-dimensional smooth-anomaly diagnostic, not a sharp-interface or field-scale inversion test.

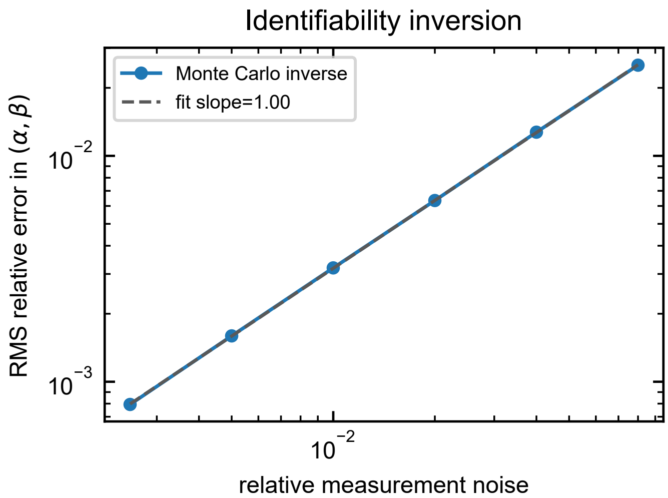

Figure 8: Identifiability inversion using the convention $\gamma_d = 1-\alpha/\beta$ from Proposition 4.12. RMS relative error in the recovered (α, β) versus relative measurement noise on (ϕ, γ_d), averaged over four admissible order pairs and 2000 trials each.

7.7 Experiment E: identifiability inversion

We test the identifiability result of Section 4.5 numerically. From a true pair (α, β) we compute the attenuation angle and the velocity-dispersion exponent $\gamma_d = 1 - \alpha/\beta$, add independent Gaussian relative noise, and recover (α, β) from the closed inverse of Proposition 4.14. Averaging over four representative order pairs and 2000 trials each, the RMS recovery error scales approximately linearly with the input noise (Figure 8). This confirms that attenuation and dispersion together break the two-order degeneracy (11) in the controlled diagnostic setting. It should not be read as a field inversion experiment: in field data the usable bandwidth is finite, high-frequency phase-velocity dispersion can be substantially noisier than the perturbative noise levels used here, and the inverse map should be regularized by spatial smoothness, prior bounds on admissible orders, and uncertainty propagation before being used for Q compensation or imaging.

Table 2: Illustrative use of the fixed-band heterogeneity indicator. The numerical cutoffs are reporting bins for numerical diagnostics and theorem use, not universal geological or rock-physics thresholds; they should be recalibrated for a chosen bandwidth, wavelength and residual gate.

Indicator regime	Mathematical reading	Modelling decision
$\mathcal{I}_U < 0.05$	Strong scale separation on the fixed band; Theorem 5.15 is expected to be a conservative local guide.	Frozen or smoothly varying local constant-Q interpretation is usually defensible after residual checks.
$0.05 \le \mathcal{I}_U < 0.2$	Transitional WKB regime; gradient terms may be visible and frequency-window dependence should be reported.	Use local windows and report estimator residuals; avoid replacing the region by a single averaged order without an error check.
$\mathcal{I}_U \ge 0.2$ or an order jump	The small-gradient premise is weak or absent; Section 6 predicts possible order-one frozen-Q error.	Treat regional averaging as uncontrolled; use interface-aware, regularized, or nonlocal modelling instead.

7.8 Geophysical use of the criterion

The practical output of the analysis is a screening rule rather than a full inversion workflow. Given order profiles $\alpha(x), \beta(x)$, a velocity scale $c(x)$, and a seismic band $[\omega_1, \omega_2]$, the user should first check the passive-cone margin $\alpha + \beta > 2 + \eta$. The next diagnostic is the fixed-band heterogeneity indicator

$$\mathcal{I}_U = \left(\|\nabla\alpha\|_{L^\infty(U)} + \|\nabla\beta\|_{L^\infty(U)}\right) \sup_{U\times[\omega_1,\omega_2]} |k(x,\omega)|^{-1}.$$

Small $\mathcal{I}_U$ means that the frozen constant-Q law is expected to remain locally stable, with $Q(x,\omega)$ close to $Q_0(x)$ in the closed corridors of Theorem 5.15 and in the conditional reduction of Proposition 5.5. Large $\mathcal{I}_U$, or an order jump, means that regional averaging should be treated as a modelling approximation with possible order-one frozen-Q error rather than as a controlled local medium.

Fixed-band local-Q admissibility screen. The criterion can be used as the following four-step diagnostic workflow:

1. choose the spatial window U and the seismic band $[\omega_1, \omega_2]$;
2. check the passive margin $\alpha(x) + \beta(x) > 2 + \eta$ and branch consistency on U;
3. estimate the local wavenumber floor and compute $\mathcal{I}_U$;
4. classify the region as stable, transitional, or uncontrolled using Table 2, and use regional averaging only in windows that pass the smooth fixed-band screen.

The criterion may serve as a stability screen for future Q-compensated imaging workflows: local constant-Q compensation is best justified in smooth regions with small $\mathcal{I}_U$, while sharp contrasts require explicit interface, transmission, or regularized nonlocal modelling. The paper does not provide an imaging algorithm; it provides the branch and gradient criterion that such algorithms should respect.

8 Discussion and outlook

We have given a branch-resolved microlocal footing to a variable-order near-constant-Q regime. The frozen model has an exact constant-Q law and a two-order manifold. Smooth order variation produces an explicit fixed-band WKB deviation controlled by $\|\nabla\alpha\| + \|\nabla\beta\|$, while order averaging can fail at order one across sharp contrasts. These statements are forward-model diagnostics. The paper should be read as a local fixed-band microlocal criterion, not as a global propagation theory: it does not prove transmission through sharp order jumps, caustic-crossing parametrices, field-scale inversion stability, or a compensated-imaging algorithm.

Finite-dimensional requested-time Mittag–Leffler evaluators for prescribed self-adjoint semidiscrete operators are developed separately in the companion EarthArXiv preprint by Hu et al. (2026), and are related only through the frozen modelling context; they are distinct from the continuous microlocal operator considered here. The present WKB, identifiability, and averaged-order results neither require nor use a numerical convergence bridge from such projected matrices. Because the exact frozen-Q locus and its gradient corrections make the local attenuation–dispersion relation explicit, the criterion developed here may serve as a stability screen for future constant-Q deconvolution or Q-compensated imaging workflows, especially by identifying when a smooth local approximation is defensible and when sharp contrasts make regional averaging uncontrolled.

Relation to classical constant-Q models. The theorem does not replace Kjartansson-type constant-Q theory. In frozen coefficients it recovers the same power-law mechanism through the selected complex branch. Its contribution is narrower and more diagnostic: it identifies which two-order branches realize a prescribed Q_0, which additional dispersion datum is needed to identify the pair (α, β), and how much smooth spatial variation can be admitted before the local constant-Q interpretation becomes a fixed-band approximation rather than an exact law.

Causality and global scope. The Kramers–Kronig statement in Section 4 is a frozen-branch result. For spatially variable orders, the WKB construction preserves the causal-passive branch only locally and perturbatively along admissible rays. We do not prove a global retarded Green's function, causal semigroup, or nonlocal transmission theorem for strongly heterogeneous or discontinuous media. This is why the multidimensional part of the result is stated as a local fixed-band reduction and then closed only in the corridors of Theorem 5.15, rather than as a global wave-propagation theory.

Failure modes of the criterion. The fixed-band criterion should be rejected, or at least reported as uncontrolled, in the following situations: a passive-branch margin is lost; the frequency band is so wide that the logarithmic constants of Lemma 2.7 dominate the gradient scale; attenuation is no longer weak in the multidimensional corridor and no complex caustic-free phase is supplied; α or β has a jump or rapid transition at the wavelength scale; the local plane-wave residual in Hypothesis 5.1 is large; or the observed attenuation and dispersion slopes are inconsistent with the two-order manifold and the branch selected in Section 4. These cases are not counterexamples to Theorem 5.15; they are outside its input contract.

Several directions are natural. The two-order degeneracy (11) suggests an inverse problem: recovering (α, β), or the quality-factor profile, from data. A fully global version of the conditional reduction in Proposition 5.5 would require a variable-order complex parametrix with explicit remainder control through caustics, boundary layers, and lower-frequency regimes. Two problems are left open in particular: (i) such a multidimensional variable-order parametrix beyond the high-Q corridor of Proposition 5.12 and through caustics; and (ii) a rigorous *nonlocal transmission* analysis at a sharp order interface, which Section 6 only diagnoses through the averaged-order error. Lemmas 2.4-2.5 and Appendix A provide only the logarithmic symbol estimates needed for the local fixed-band WKB statement; neither open problem is delegated to the companion manuscript.

For completeness we record proofs of the two symbol estimates used in the main text; they make the paper self-contained modulo the standard pseudodifferential parametrix construction.

Proof of Lemma 2.4. Write $m(x,\xi) = \langle\xi\rangle^{\beta(x)} = e^{\beta(x)L}$ with $L := \log\langle\xi\rangle$, which does not depend on x. Then $\partial_{x_j} m = (\partial_{x_j}\beta)Lm$, so the claim holds for $|\gamma| = 1$ with $P_{e_j} = (\partial_{x_j}\beta)L$, a degree-one polynomial in L. Inductively, if $\partial_x^\gamma m = P_\gamma(x,L)m$ with $\deg_L P_\gamma = |\gamma|$, then

$$\partial_{x_j}(P_\gamma m) = \big(\partial_{x_j} P_\gamma + P_\gamma(\partial_{x_j}\beta)L\big)\, m,$$

and the bracket has L-degree $|\gamma|+1$. The coefficients are polynomial in the derivatives of β by construction. The bound $|\partial_x^\gamma \langle\xi\rangle^\beta| \le C_\gamma \langle\xi\rangle^\beta (\log\langle\xi\rangle)^{|\gamma|}$ follows, and multiplying by $c^2(x) \in C^1$ and applying ∂_ξ^δ, which gains $\langle\xi\rangle^{-|\delta|}$, gives $c^2\langle\xi\rangle^{\beta(x)} \in S_{\mathrm{var}}^{\beta(\cdot)}$. □

Proof of Lemma 2.5. With $L = \log\langle\xi\rangle \ge 0$, the function $L^k e^{-\varepsilon L}$ attains its maximum over $L \ge 0$ at $L = k/\varepsilon$, with value $(k/(e\varepsilon))^k$. Hence $L^k \le (k/(e\varepsilon))^k e^{\varepsilon L} = (k/(e\varepsilon))^k \langle\xi\rangle^\varepsilon$; multiplying by $\langle\xi\rangle^{\beta(x)}$ gives the stated inequality, uniformly in x since the constant is x-independent. The inclusion $S_{\mathrm{var}}^{\beta(\cdot)} \subset S_{1,0}^{\beta_+ + \varepsilon}$ is immediate, and the classical Calderón-Vaillancourt and parametrix theory then apply with an ε-loss in the order, which does not affect the leading-order asymptotics used in Proposition 5.5. □

A The phase-space integral and the transport coefficients

A.1 A phase-space integral

The following elementary integral underlies the deviation analysis and the corresponding frozen-symbol spectral calculations. For $b, \Lambda > 0$, $\beta \in (0,2)$, and with $\rho = (\Lambda/b)^{1/\beta}$,

$$\begin{aligned}\int_{\mathbb{R}^d} (\Lambda - b|\xi|^\beta)_+\, d\xi &= d\omega_d \int_0^\rho (\Lambda - br^\beta) r^{d-1}\, dr \\ &= \omega_d \left[\Lambda\rho^d - \frac{db\rho^{d+\beta}}{d+\beta}\right] \\ &= \omega_d \frac{\beta}{d+\beta} \Lambda(\Lambda/b)^{d/\beta},\end{aligned}$$

using $b\rho^\beta = \Lambda$.

A.2 The transport coefficients

From (21)-(22), and using the first transport equation (25) now derived from the expansion (23) in Section 5.2, the bracketed coefficient is, to leading order in the small parameters $\nabla\alpha, \nabla\beta$,

$$\delta\kappa_{\mathrm{vo}} = -\frac{(\partial_x\alpha)(-i\omega)^\alpha \log(-i\omega) + c^2(x)(\partial_x\beta)\kappa^{\beta(x)}\log\kappa}{\beta(x)c^2(x)\kappa^{\beta(x)-1}} + \text{lower-order transport terms},$$

where $\log\kappa$ is evaluated on the causal-passive branch fixed in Lemma 4.1. Using the eikonal relation (20), the numerator is proportional to $\kappa^{\beta(x)}$ and division by $\partial_\kappa[c^2(x)\kappa^{\beta(x)}] = \beta(x)c^2(x)\kappa^{\beta(x)-1}$ leaves a first correction of size

$$|\delta\kappa_{\mathrm{vo}}| \le C|\kappa| \left(|\partial_x\alpha|\, |\log\omega| + |\partial_x\beta|\, |\log\kappa|\right).$$

After normalization by the leading wavenumber and conversion from κ to $Q = \kappa_R/(2\kappa_I)$ on the passive cone, this gives the structure of (27). The constants depend only on the admissible ranges of α, β, c and on the fixed frequency band.

A.3 Derivation of the leading coefficient (40)-(41)

Derivation of (40)–(41). Starting from B.2 and the eikonal $(-i\omega)^\alpha = -c^2\kappa^\beta$,

$$(\partial_x\alpha)(-i\omega)^\alpha \log(-i\omega) = -(\partial_x\alpha)\, c^2\kappa^\beta \log(-i\omega),$$

so the B.2 numerator equals $c^2\kappa^\beta\big[-(\partial_x\alpha)\log(-i\omega) + (\partial_x\beta)\log\kappa\big] = -c^2\kappa^\beta B$. Dividing by $\beta c^2\kappa^{\beta-1}$ gives (40). Writing $\delta\kappa/\kappa = B/\beta$ and taking imaginary parts with $\log(-i\omega) = \log\omega - i\pi/2$ and $\log\kappa = \log|\kappa| + i\phi$ yields $\delta\phi = \beta^{-1}\Im B = -\beta^{-1}(\frac{\pi}{2}\partial_x\alpha + \phi\,\partial_x\beta)$; composing with $dQ_0/d\phi = -\frac{1}{2}\csc^2\phi$ gives (41). The coefficient is a nonzero linear functional of $(\partial_x\alpha, \partial_x\beta)$ on the admissible set; hence the response is locally first order whenever this functional does not vanish, and the lower bound (42) holds under the non-cancellation condition stated in Proposition 5.16. $\square$

B Numerical methods and reproducibility

All direct variable-order experiments use the Kohn–Nirenberg spectral discretization of Section 7. For a spatial order graded in one direction, $\beta = \beta(x_1)$, and an isotropic symbol, transverse Fourier modes decouple. Each reported oblique-mode experiment therefore reduces to a dense linear solve on the x_1-line for the chosen transverse wavenumber k_2, with the two-dimensional symbol $|k| = \sqrt{k_1^2 + k_2^2}$. This is a modal two-dimensional validation of the symbol and branch formula, not a fully nonseparable simulation with $\beta = \beta(x_1, x_2)$.

Outgoing waves are absorbed by a quadratic sponge layer $\mathrm{i}\gamma(x_1)$ of width d_{abs} at each end. The field is launched by a narrow Gaussian soft source just inside the left layer. The complex wavenumber is extracted by a least-squares fit of $\log v$ over an interior window; source-adjacent points, absorbing-layer points, and points within two fitting-window widths of the artificial boundaries are excluded from quantitative averages. The known k_2 is then used to reconstruct $|k|$ and Q. Unless stated otherwise, $\alpha = 1.8$, $c = 1$, $\omega = 1$, $k_2 = 0.30$, grid $N = 1024$ on $[0, 80]$, absorbing width $d_{\mathrm{abs}} = 16$, and sponge strength $\gamma_{\max} = 8$.

Experiment	Key parameters	Output
Homogeneous (7.1, 7.6)	$\beta \in \{1.1, 1.5, 1.9\}$	Q_{num} vs. (10)
Two-layer (7.2, 7.6)	$\beta_0 = 1.9$, $\beta_1 = 1.1$, tanh width 1.5	per-layer Q, $\bar{Q}_0$
WKB coefficient diagnostic (7.6)	Appendix B, $\alpha = 1.8$, representative $\beta = 1.5$	linear coefficient vs. $\lVert\nabla\beta\rVert_\infty$
Angle sweep (7.6)	$k_2 \in \{0, 0.2, 0.4, 0.6\}$	dimension-independence
Frequency envelope (7.6)	fixed-band symbolic scale	normalized $\log\langle k\rangle/\langle k\rangle$
Nonseparable 2D scattering (7.7)	compact $\beta(x, y)$ contrast, direct Kohn–Nirenberg matrix	scattered-field response scaling
Smooth low-Q anomaly (7.7)	embedded $\beta(x, y)$ anomaly, direct Kohn–Nirenberg matrix	wavefield snapshot and windowed $Q_{\mathrm{num}}(x, y)$ samples
Identifiability (7.8)	2000 trials, noise $\eta \le 5\%$	RMS recovery error

The computations are deterministic (a fixed random seed is used for the identifiability Monte Carlo) and depend only on `numpy`, `matplotlib`, and `Pillow`. The supplementary script `P1_reproduce_figures.py` regenerates Figures 4–5 and the identifiability Figure 8, together with their CSV/NPZ source data. The script `P1_2D_variable_order_solver.py` regenerates Figure 6 and the associated two-dimensional scattering data. The script `P1_2D_lowQ_anomaly.py` regenerates Figure 7 and its accepted local-Q samples. Earlier oblique-mode and k-Wave diagnostics are supplied as separate scripts and should be treated as supporting diagnostics. Figure 6 is a reproducible nonseparable two-dimensional finite-dimensional scattering diagnostic. It checks matrix assembly, algebraic residuals, and local

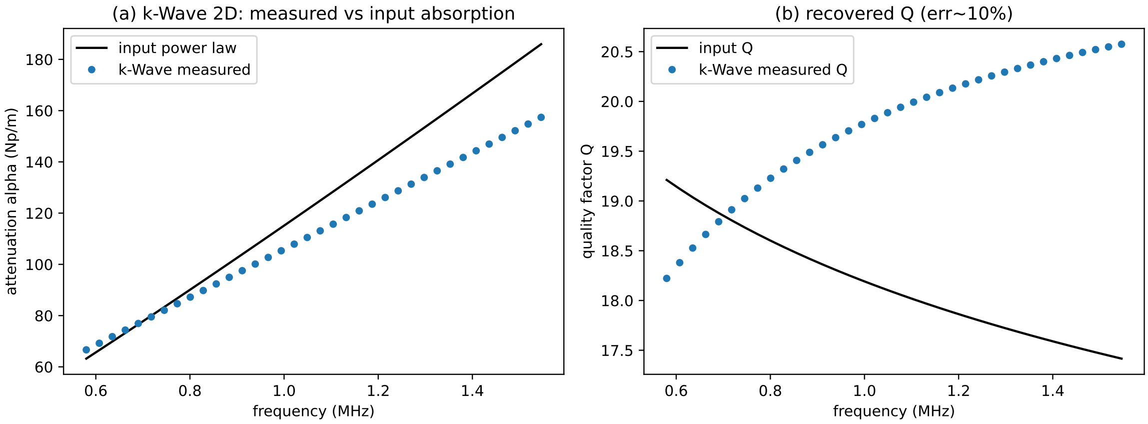

Figure 9: Supporting 2D cross-model check with the k-Wave pseudospectral solver of Treeby and Cox (2010) (grid 384^2, power-law exponent $y = 1.1$, ten-receiver profile, time-windowed spectral ratio). (a) Attenuation $\alpha(f)$: k-Wave measurement (markers) versus the prescribed power law (line). (b) Quality factor: k-Wave extraction versus the prescribed Q; agreement within $\sim 10\%$, consistent with point-source spectral-ratio accuracy in field practice. This figure supports only the frozen constant-order background and is not used as evidence for the variable-order WKB theorem.

parameter response on the reported grid; it establishes neither grid convergence nor a pointwise local-Q inversion.

C External constant-order sanity check, not evidence for the theorem

The formula (10) and the constant-Q framework are not tied to one dimension in the frozen case. As an external consistency check for the constant-order power-law setting, we used k-Wave (Treeby and Cox, 2010), a widely used pseudospectral time-domain package whose power-law absorption is implemented through a fractional Laplacian. This is a cross-model check only: it is not part of the evidence for the variable-order WKB formula and it does not verify the Kohn–Nirenberg variable-order operator. We ran a 2D viscoacoustic simulation (grid 384^2, sound speed 1500 m s^{-1}, power-law exponent $y = 1.1$) with a broadband point source and ten receivers along a profile, and recovered the quality factor by the time-windowed spectral-ratio method (Tonn, 1991).

The agreement is within $\sim$ 10% across the source bandwidth, which is expected for a point-source spectral-ratio estimate. The check is therefore retained as background geophysical context rather than a main validation axis.

Data and code availability

No external empirical datasets were used. The code and source data for the deterministic diagnostics reported here are archived on Zenodo at https://doi.org/10.5281/zenodo.21486530 (doi:10.5281/zenodo.21486530); no proprietary field data are required for the theorem or for reproducing the diagnostic figures. In particular, `P1_reproduce_figures.py` generates the corrected formula-level Figures 4–5, the identifiability Figure 8, and the corresponding CSV/NPZ data files. The independent script `P1_2D_variable_order_solver.py` assembles the small-grid nonseparable two-dimensional Kohn–Nirenberg operator, generates Figure 6, and writes the associated NPZ/JSON source data. The script `P1_2D_lowQ_anomaly.py` generates

Figure 7 and `P1_2D_lowQ_anomaly_summary.json`. The k-Wave consistency script is optional and requires a separate k-Wave Python installation; it is not used as evidence for the variable-order WKB theorem.

Funding and competing interests

No specific funding was received for this work. The authors declare no competing interests. All authors contributed to conceptualization, mathematical analysis, manuscript writing, and revision, and approved the final manuscript. AI tools were used to assist with language editing, consistency checks, code organization, and submission-package preparation; the authors independently verified the mathematical claims, references, numerical outputs, and final wording.

Acknowledgements

The variable-order symbol estimates used in this paper are recorded self-containedly in Lemmas 2.4-2.5 and Appendix A. Broader spectral applications of related variable-order operators are left to separate work.

References

Caffarelli, L. & Silvestre, L., 2007. *An extension problem related to the fractional Laplacian*, Communications in Partial Differential Equations, **32**(8), 1245–1260, doi:10.1080/03605300600987306.

Caputo, M., 1967. *Linear models of dissipation whose Q is almost frequency independent–II*, Geophysical Journal of the Royal Astronomical Society, **13**(5), 529–539, doi:10.1111/j.1365-246X.1967.tb02303.x.

Carcione, J. M., Cavallini, F., Mainardi, F., & Hanyga, A., 2002. *Time-domain modeling of constant-Q seismic waves using fractional derivatives*, Pure Appl. Geophys., **159**, 1719–1736, doi:10.1007/s00024-002-8705-z.

Chechkin, A. V., Gorenflo, R., & Sokolov, I. M., 2005. *Fractional diffusion in inhomogeneous media*, Journal of Physics A: Mathematical and General, **38**(42), L679–L684, doi:10.1088/0305-4470/38/42/L03.

Chen, W. & Holm, S., 2004. *Fractional Laplacian time-space models for linear and nonlinear lossy media exhibiting arbitrary frequency power-law dependency*, Journal of the Acoustical Society of America, **115**(4), 1424–1430, doi:10.1121/1.1646399.

Coimbra, C. F. M., 2003. *Mechanics with variable-order differential operators*, Annalen der Physik, **12**(11–12), 692–703, doi:10.1002/andp.200310032.

Darve, E., D'Elia, M., Garrappa, R., Giusti, A., & Rubio, N. L., 2022. *On the fractional Laplacian of variable order*, Fract. Calc. Appl. Anal., **25**, 15–28, doi:10.1007/s13540-021-00003-1.

Gorenflo, R., Kilbas, A. A., Mainardi, F., & Rogosin, S. V., 2020. *Mittag-Leffler Functions, Related Topics and Applications*, 2nd edn, Springer, Berlin, doi:10.1007/978-3-662-61550-8.

Holm, S. & Näsholm, S. P., 2011. *A causal and fractional all-frequency wave equation for lossy media*, Journal of the Acoustical Society of America, **130**(4), 2195–2202, doi:10.1121/1.3631626.

Hu, N., Huang, C., Li, S., & Hu, C., 2026. *History-free spectral modelling of fractional seismic attenuation on fixed self-adjoint operators*, EarthArXiv preprint, doi:10.31223/X5ZR3T.

Hörmander, L., 2007. *The Analysis of Linear Partial Differential Operators III: Pseudo-Differential Operators*, Classics in Mathematics, Springer, Berlin, doi:10.1007/978-3-540-49938-1.

Jia, J., Jiang, C., Li, Y., Liu, M., & Qiu, W., 2025. *Variable-order fractional wave equation: analysis, numerical approximation, and fast algorithm*, CoRR, abs/2511.06014, doi:10.48550/arXiv.2511.06014.

Kjartansson, E., 1979. *Constant Q-wave propagation and attenuation*, J. Geophys. Res., **84**, 4737–4748, doi:10.1029/JB084iB09p04737.

Kwaśnicki, M., 2017. *Ten equivalent definitions of the fractional Laplace operator*, Fractional Calculus and Applied Analysis, **20**(1), 7–51, doi:10.1515/fca-2017-0002.

Leopold, H.-G., 1989. *On Besov spaces of variable order of differentiation*, Zeitschrift für Analysis und ihre Anwendungen, **8**(1), 69–82, doi:10.4171/ZAA/337.

Leopold, H.-G. & Schrohe, E., 1993. *Spectral invariance for algebras of pseudodifferential operators on Besov–Triebel–Lizorkin spaces*, Manuscripta Mathematica, **78**(1), 99–110, doi:10.1007/BF02599303.

Lorenzo, C. F. & Hartley, T. T., 2002. *Variable order and distributed order fractional operators*, Nonlinear Dynamics, **29**(1–4), 57–98, doi:10.1023/A:1016586905654.

Robertsson, J. O. A., Blanch, J. O., & Symes, W. W., 1994. *Viscoelastic finite-difference modeling*, Geophysics, **59**(9), 1444–1456, doi:10.1190/1.1443701.

Samko, S. G. & Ross, B., 1993. *Integration and differentiation to a variable fractional order*, Integral Transforms and Special Functions, **1**(4), 277–300, doi:10.1080/10652469308819027.

Shubin, M. A., 2001. *Pseudodifferential Operators and Spectral Theory*, 2nd edn, Springer, Berlin, doi:10.1007/978-3-642-56579-3.

Stein, E. M., 1993. *Harmonic Analysis: Real-Variable Methods, Orthogonality, and Oscillatory Integrals*, Princeton University Press, Princeton, doi:10.1515/9781400883929.

Sun, H., Chen, W., & Chen, Y., 2009. *Variable-order fractional differential operators in anomalous diffusion modeling*, Physica A: Statistical Mechanics and its Applications, **388**(21), 4586–4592, doi:10.1016/j.physa.2009.07.024.

Szabo, T. L., 1994. *Time domain wave equations for lossy media obeying a frequency power law*, Journal of the Acoustical Society of America, **96**(1), 491–500, doi:10.1121/1.410434.

Tonn, R., 1991. *The determination of the seismic quality factor Q from VSP data: a comparison of different computational methods*, Geophys. Prospect., **39**, 1–27, doi:10.1111/j.1365-2478.1991.tb00298.x.

Treeby, B. E., & Cox, B. T., 2010. *Modeling power law absorption and dispersion for acoustic propagation using the fractional Laplacian*, J. Acoust. Soc. Am., **127**, 2741–2748, doi:10.1121/1.3377056.

Zhu, T., & Carcione, J. M., 2014. *Theory and modelling of constant-Q P- and S-waves using fractional spatial derivatives*, Geophys. J. Int., **196**, 1787–1795, doi:10.1093/gji/ggt483.

Zhu, T., & Harris, J. M., 2014. *Modeling acoustic wave propagation in heterogeneous attenuating media using decoupled fractional Laplacians*, Geophysics, **79**, T105–T116, doi:10.1190/geo2013-0245.1.